Complete mapping of crystallization pathways during cholesterol precipitation from model bile: influence of physical–chemical variables of pathophysiologic relevance and identification of a stable liquid crystalline state in cold, dilute and hydrophilic bile salt-containing systems[1]

David Q-H. Wang and Martin C. Carey[2]

Department of Medicine, Gastroenterology Division, Brigham and Women's Hospital, Harvard Medical School and Harvard Digestive Diseases Center, Boston, MA 02115

Abstract Using complementary physical–chemical techniques we defined five different crystallization pathways as functions of time (30 days) and increasing lecithin (egg yolk) content in pathophysiologically relevant model biles supersaturated (cholesterol saturation indices, 1.2–2.7) by dilution of ≈29 g/dl bile salt–lecithin–cholesterol micellar solutions. As evidenced by quasi-elastic light-scattering spectroscopy, supersaturation was heralded by the appearance of unilamellar vesicles. With the lowest lecithin contents, arc-like crystals with habit and density (d 1.030 g/mL) consistent with anhydrous cholesterol appeared first and evolved via helical and tubular crystals to form plate-like cholesterol monohydrate crystals (d 1.045 g/mL). With higher lecithin fractions, cholesterol monohydrate crystals appeared earlier than arc and other transitional crystals. With typical physiological lecithin contents, early liquid crystals (d 1.020 g/mL) were followed by cholesterol monohydrate crystals and subsequent appearances of arc and other intermediate crystals. With higher lecithin contents, liquid crystals were followed by cholesterol monohydrate crystals only, and at the highest lecithin mole fractions, liquid crystals appeared that did not generate solid crystals. Added calcium increased solid crystal number in proportion to its concentration (5–20 mM) but did not influence appearance times, crystallization pathways, or micellar cholesterol solubilities. Decreases in temperature (37° → 4°C), total lipid concentration (7.3 → 2.4 g/dL), and bile salt hydrophobicity (3α,12α → 3α,7α → 3α,7α,12α → 3α,7β hydroxylated taurine conjugates) progressively shifted all crystallization pathways to lower lecithin contents, retarded crystallization, and decreased micellar cholesterol solubilities. The lecithin content of mother biles decreased markedly during crystallization especially where liquid crystals were a coexisting phase at equilibrium. This systematic study provides a framework for understanding cholesterol crystallization in human and animal biles and for examining factors that influence the kinetics of phase separation.–**Wang, D. Q-H., and M. C. Carey.** Complete mapping of crystallization pathways during cholesterol precipitation from model bile: influence of physical–chemical variables of pathophysiologic relevance and identification of a stable liquid crystalline state in cold, dilute and hydrophilic bile salt-containing systems. *J. Lipid Res.* 1996. **37:** 606–630.

Supplementary key words gallstones • phospholipid • lecithin • liquid crystals • crystal habits • crystal density • phase diagrams • microscopy • quasi-elastic light-scattering • calcium

In cholesterol (Ch) gallstone formation, supersaturated bile is followed by precipitation of cholesterol monohydrate (ChM) crystals which agglomerate to form macroscopic gallstones (1). Microscopic detection of ChM crystals in human bile was proposed as the rate-limiting step in gallstone formation (2, 3) and is commonly but erroneously called "nucleation" (2). Nevertheless, the overall processes can be subdivided into true

Abbreviations: Ch, cholesterol; ChM, cholesterol monohydrate; QLS, quasi-elastic light-scattering spectroscopy; TC, taurocholate; ACh, anhydrous cholesterol; L, egg yolk lecithin; HPLC, high performance liquid chromatography; BS, bile salt; GC, glycocholate; GCDC, glycochenodeoxycholate; GDC, glycodeoxycholate; GLC, glycolithocholate; GLCS, glycolithocholate sulfate; TCDC, taurochenodeoxycholate; TDC, taurodeoxycholate; TLC, taurolithocholate; TLCS, taurolithocholate sulfate; TUDC, tauroursodeoxycholate; C, cholate; MBS, mixed bile salts (all as sodium salts); CSI, cholesterol saturation index; $\bar{R}_h$, mean hydrodynamic radius; [TL], total lipid concentration; d, density.

[1]This paper was presented in part at the Annual Meeting of the American Gastroenterological Association, New Orleans, LA 1994 and published as an abstract in *Gastroenterology.* 1994. **106:** A1004.

[2]To whom correspondence should be addressed at: Department of Medicine, Gastroenterology Division, Thorn 1330, Brigham and Women's Hospital, 75 Francis Street, Boston, MA 02115.

TABLE 1. Analytical lipid compositions of stock cholesterol-saturated micellar biles

Number	Mole % Ch[a]	Mole % L[a]	Mole%BS[a]	L/(L + BS)	[TL] (g/dl)	CSI[a]
1	2.70 ± 0.05	1.88 ± 0.09	95.41 ± 0.12	0.02	29.16 ± 0.46	0.91 ± 0.02
2	3.48 ± 0.15	4.79 ± 0.10	91.74 ± 0.17	0.05	28.78 ± 0.74	0.95 ± 0.03
3	4.79 ± 0.16	9.49 ± 0.22	85.72 ± 0.26	0.10	28.96 ± 0.57	0.96 ± 0.01
4	6.27 ± 0.15	14.16 ± 0.40	79.57 ± 0.49	0.15	28.89 ± 0.78	0.98 ± 0.01
5	7.39 ± 0.18	18.55 ± 0.59	74.06 ± 0.65	0.20	29.16 ± 0.54	0.96 ± 0.02
6	8.07 ± 0.47	22.87 ± 0.84	69.06 ± 0.85	0.25	29.24 ± 0.48	0.93 ± 0.02
7	8.83 ± 0.59	26.84 ± 0.77	64.32 ± 1.03	0.30	29.42 ± 0.48	0.93 ± 0.02
8	9.60 ± 0.06	31.55 ± 0.48	58.84 ± 0.78	0.35	28.95 ± 0.97	0.98 ± 0.01
9	9.48 ± 0.06	36.39 ± 0.45	54.13 ± 0.40	0.40	28.72 ± 0.40	0.98 ± 0.01
10	9.23 ± 0.12	41.50 ± 0.38	49.26 ± 0.39	0.45	29.23 ± 0.47	0.97 ± 0.01
11	8.97 ± 0.07	45.79 ± 0.51	45.24 ± 0.49	0.50	29.33 ± 0.53	0.98 ± 0.01
12	8.92 ± 0.04	49.04 ± 0.41	42.04 ± 0.42	0.55	29.05 ± 0.09	≈1.00[b]
13	8.42 ± 0.02	54.43 ± 0.46	37.15 ± 0.46	0.60	29.05 ± 0.20	≈1.00[b]
14	0.00	67.46 ± 0.25	32.54 ± 0.25	0.68	29.19 ± 0.19	0.00

Data expressed as mean ± SD except L/(L + BS) ratios. Abbreviations: Ch, cholesterol; L, lecithin (egg yolk); BS, bile salt; [TL], total lipid concentration; CSI, cholesterol saturation index. Values were calculated using the averages of all bile salt systems, e.g., TUDC (n = 3), TC (n = 6), TCDC (n = 4), TDC (n = 2), GC (n = 2), C (n = 2), and mixed bile salts (MBS) (n = 6). Other conditions were 0.15 M NaCl, pH = 7.0, T = 37°C.

[a]These values represent the mean CSI values of TC-, MBS-, and TCDC-L-Ch systems calculated from the critical tables (21).

[b]Even though CSI values could not be calculated for Nos. 12 and 13 because they plotted outside limits of the critical tables (21), each of these biles was isotropic microscopically.

[c]No added cholesterol.

nucleation,[3] precipitation of solid and liquid crystals (crystallization), crystal growth, crystal agglomeration, and stone growth (reviewed in ref. 4). The physical chemistry of bile and the conditions necessary for Ch gallstone formation have a thermodynamic basis in multicomponent phase diagrams of aqueous biliary lipid systems (5–7). Although quasi-elastic light-scattering spectroscopy (QLS) was shown capable of characterizing early precipitation kinetics in model bile (8), physical chemical understanding of nucleation and subsequent crystallization has been slow in progressing. High-resolution video-enhanced microscopy (9) provided evidence that Ch crystallization from supersaturated model and human bile was a sequence of vesicle formation, possibly vesicle aggregation and crystallization (9–11). More recently, Konikoff et al. (12), Chung et al. (13), and Konikoff and Carey (14) found that the earliest Ch crystals in a dilute (1.2 g/dL) model bile composed with 97.5% sodium taurocholate (TC) were long filamentous crystals that had habit, density, and X-ray spacings consistent with anhydrous cholesterol (ACh) (15). Over a period of several days, the filaments were replaced by a series of metastable intermediate needle, helical, and tube-like crystals and then classic ChM plates (12–14). These findings, taken together with the liquid crystalline pathway (9–11), drew attention to the remarkable dearth of systematic information that prevailed on Ch precipitation and crystallization in model and native biles. We have now defined five distinct Ch crystallization pathways in supersaturated model biles of pathophysiological relevance as functions of time and increasing lecithin (L) content and describe the evolution and metastabilities of intermediate as well as solid and liquid crystals. Because the model biles were followed to true equilibrium (~30 days), additional sets of phase diagrams have been developed for a number of new pathophysiological conditions. Furthermore, we studied model biles with different added Ca^{2+} concentrations to explore the effects of the principal divalent cation in bile (16) on phase equilibria as well as Ch crystallization and crystal growth rates. Our findings provide a framework for investigating the physical-chemistry and kinetics of Ch precipitation and crystal growth in native biles and the conditions necessary for stabilizing the supersaturated state.

[3]Nucleation is the condensation or aggregation process by which a propagable submicroscopic crystal or amorphous particle is formed from a supersaturated bile, i.e., from a micelle plus vesicle system. The submicroscopic crystal may or may not form on a minute amount of substance that acts as a nucleus for subsequent crystal growth. In the context of model systems of bile, because supersaturation involves a second vesicle phase ab initio, we can loosely refer to multilamellar vesicles (or liquid crystals) as nucleated particles also.

MATERIALS AND METHODS

Chemicals

Grade A TC, (Sigma Chemical Co., St. Louis, MO), was recrystallized (17) and found to be > 99% pure by high performance liquid chromatography (HPLC). Other conjugated bile salts (BS), i.e., glycocholate (GC), glycochenodeoxycholate (GCDC), glycodeoxycholate (GDC), glycolithocholate (GLC), glycolithocholate sulfate (GLCS), taurochenodeoxycholate (TCDC), taurodeoxycholate (TDC), taurolithocholate (TLC), taurolithocholate sulfate (TLCS), tauroursodeoxycholate (TUDC), as well as unconjugated cholate (C), all sodium salts, were purchased from Sigma Chemical Co. and Calbiochem-Behring (San Diego, CA). Purity of individual BS by HPLC was generally > 98%, with TLCS being > 96%, whereas by thin-layer chromatography (butanol–acetic acid–water 10:1:1, vol/vol/vol), all BS were > 98% pure. Ch was from Nu-Chek Prep Inc., (Elysian, MN) and was ≈98% pure by HPLC (isopropanol–acetonitrite 1:1 by vol (18)) and grade I egg yolk L (Lipid Products, South Nutfield, Surrey, UK) was > 99% pure by thin-layer chromatography (chloroform–methanol–water 65:25:4 vol/vol/vol) (19) and HPLC. Standards used were *sn*-2 oleoyl and linoleoyl lysolecithins from Serdery Research Laboratories (London, Ontario, Canada). All other chemicals and solvents were American Chemical Society (ACS) or reagent grade quality (Fisher Scientific Co., Medford, MA). $CaCl_2$ was purchased from Orion Research Inc. (Boston, MA). ACS grade NaCl was roasted at 600°C for 4 h in a muffle furnace to oxidize and remove organic impurities. As authentic crystalline standards, ChM and ACh crystals were prepared by precipitation from 95% EtOH and 100% acetic acid, respectively (20).

Preparation of model biles

Stock micellar biles (**Table 1**) were prepared (7) with L and Ch and either a single BS (see Materials), or a physiological mixture of BS (MBS), containing C:CDC:DC:LC:LCS in a ratio of 12:12:8:0.3:1 (22, 23) with a G:T conjugate composition of 2:1. After coprecipitation from $CHCl_3$–MeOH 2:1 (vol/vol), lipid mixtures were dried under a stream of N_2 and at reduced pressure to constant weight. Each lipid film was dissolved in aqueous 0.15 M NaCl plus 3 mM NaN_3 (as an antimicrobial agent) adjusted with a few μL of 1 M NaOH to pH 7.0. To ensure complete BS ionization, stock biles containing GC or C alone were reconstituted in aqueous 33 mM NaH_2PO_4/Na_2HPO_4 plus 3 mM NaN_3 at pH 8.0 and 9.0, respectively, and sufficient NaCl to give the appropriate ionic strength. Tubes were sealed with Teflon-lined screw caps under a blanket of N_2 and vigorously vortex-mixed for a few min. To avoid persist-

TABLE 2. Analytical lipid compositions of stock cholesterol-supersaturated biles

Number	Mole % Ch	Mole % L	Mole % BS	$L_t/(L + BS)$	[TL] (g/dl)	CSI[a]
1	7.79 ± 0.15	4.60 ± 0.04	87.61 ± 0.16	0.05	28.96 ± 0.68	2.13 ± 0.02
2	9.83 ± 0.17	8.98 ± 0.08	81.19 ± 0.22	0.10	29.07 ± 0.74	1.97 ± 0.02
3	10.74 ± 0.30	13.29 ± 0.20	75.98 ± 0.49	0.15	29.19 ± 0.45	1.68 ± 0.02
4	13.84 ± 0.13	13.12 ± 0.37	73.04 ± 0.27	0.15	29.36 ± 0.65	2.16 ± 0.03
5	10.80 ± 0.11	17.39 ± 0.42	71.80 ± 0.35	0.20	29.08 ± 0.81	1.40 ± 0.01
6	14.30 ± 0.12	21.33 ± 0.20	64.37 ± 0.19	0.25	29.46 ± 0.13	1.63 ± 0.03
7	12.89 ± 0.11	26.09 ± 0.11	61.03 ± 0.11	0.30	29.07 ± 0.55	1.36 ± 0.02
8	17.89 ± 0.11	28.47 ± 0.35	53.64 ± 0.32	0.35	29.24 ± 0.41	1.83 ± 0.02
9	14.28 ± 0.13	34.33 ± 0.41	51.45 ± 0.41	0.40	29.03 ± 0.54	1.47 ± 0.03
10	19.14 ± 0.18	36.18 ± 0.18	44.68 ± 0.27	0.45	29.00 ± 0.60	2.02 ± 0.02
11	11.33 ± 0.07	39.86 ± 0.06	48.81 ± 0.12	0.45	28.94 ± 0.43	1.20 ± 0.02
12	13.27 ± 0.21	39.01 ± 0.19	47.72 ± 0.20	0.45	29.34 ± 0.62	1.40 ± 0.02
13	14.29 ± 0.13	38.34 ± 0.16	47.37 ± 0.18	0.45	29.38 ± 0.43	1.51 ± 0.03
14	11.25 ± 0.11	44.38 ± 0.26	44.37 ± 0.33	0.50	29.25 ± 0.73	1.23 ± 0.02
15	15.87 ± 0.10	41.92 ± 0.39	42.21 ± 0.40	0.50	29.43 ± 0.21	1.73 ± 0.01
16	19.22 ± 0.16	40.19 ± 0.18	40.60 ± 0.16	0.50	29.04 ± 0.89	2.10 ± 0.02

Data expressed as mean ± SD except $L_t/(L + BS)$ ratios. See footnotes of Table 1 for list of abbreviations and other conditions. These values were calculated for all bile salt systems, e.g., TUDC, TC, TCDC, TDC, GC, C, and MBS (n = 2 for each).
[a]Mean CSI values of TC-, MBS-, and TCDC-L-Ch systems calculated from the critical tables (21).

TABLE 3. Analytical lipid compositions of the MBS-L-Ch model bile systems with and without calcium

	Day 0[a]					30 Days[a]				
Number	Mole%Ch	Mole%L	MoleBS	[TL] 9g/dl)	CSI	Mole%Ch	Mole%L	Mole%BS	[TL] (g/dl)	CSI
Without calcium										
1	2.71	1.79	95.50	7.18	1.30	2.03	1.46	96.51	6.25	0.99
2	3.38	4.81	91.81	6.94	1.23	2.50	4.87	92.63	6.45	0.92
3	4.99	9.33	85.68	6.93	1.30	3.11	8.46	88.43	6.13	0.91
4	6.35	14.62	79.03	6.75	1.27	4.08	11.03	84.89	6.12	1.00
5	7.52	18.94	73.54	6.75	1.24	4.95	16.00	79.05	5.86	0.95
6	8.12	22.51	69.39	7.21	1.18	6.00	20.35	73.65	5.96	0.98
7	9.15	27.20	63.65	7.12	1.21	6.80	24.80	68.40	6.02	0.97
8	9.58	33.12	57.30	6.85	1.23	7.64	30.56	61.80	6.17	1.00
9	9.44	36.71	53.85	7.11	1.22	7.48	35.72	56.80	6.14	0.98
10	9.13	41.92	48.95	7.19	1.21	7.62	39.50	52.88	6.33	1.01
Mean ± SD				7.00 ± 0.18	1.24 ± 0.04				6.14±0.17	0.97 ± 0.03
Calcium, 10mM										
1	3.39	4.71	91.89	7.44	1.22	2.49	4.19	93.32	6.13	0.97
2	6.10	14.05	79.86	7.39	1.22	4.10	10.93	84.96	6.50	1.00
3	8.33	22.91	68.76	7.38	1.19	6.05	19.81	74.14	6.56	0.98
4	9.09	27.59	63.32	7.37	1.18	6.82	23.28	69.89	6.22	1.00
Mean ± SD				7.40 ± 0.03	1.20 ± 0.02				6.35 ± 0.21	0.99 ± 0.01
Calcium, 20 mM										
1	3.44	4.55	92.01	7.48	1.25	2.54	4.70	92.76	6.03	0.96
2	6.02	13.94	80.04	7.60	1.20	3.97	10.99	85.04	6.32	0.97
3	8.30	23.08	68.62	7.47	1.18	6.14	20.13	73.73	6.46	0.99
4	9.02	27.15	63.84	7.44	1.18	6.77	23.09	70.14	6.27	1.00
Mean ± SD				7.50 ± 0.07	1.20 ± 0.03				6.27 ± 0.18	0.98 ± 0.02

Abbreviations are as in Table 1.
[a]Other conditions were ionic strength = 0.15 M (NaCl + $CaCl_2$), pH = 7.0, T = 37°C.

ence of undissolved microcrystalline Ch, the tubes were shaken at 100 rpm for 1 h at 50°C using a model 75 Wrist Action Shaker (Burrell Corporation, Pittsburgh, PA). Because of reduced micellar Ch solubilizing capacity in the TUDC-L-Ch system (21), these mixtures were shaken vigorously for 1 h at 95°C until isotropic microscopically. Each stock solution was then microfiltered (0.22 μm filter) through a preheated Swinnex-GS filter assembly (Millipore Products Division, Bedford, MA) and a ≈0.1 ml sample was removed for analysis. To induce supersaturation, stock micellar biles (Table 1) were diluted 4-, 8-, and 12-fold with aqueous solvent at the appropriate pH. According to critical tables for the TC-L-Ch system (21), these dilutions should increase the cholesterol saturation index (CSI) to 1.17 ± 0.05, 1.40 ± 0.04, and 1.60 ± 0.05, respectively, and this constituted the initial time-points of the study (12).

To verify crystallization pathways and determine phase boundaries appreciably above the micellar phase, model biles were also prepared (7) with higher Ch contents to give supersaturated stock biles with CSIs (37°C) ranging from 1.2 to 2.1 (**Table 2**). Each model system was sealed after an N_2 purge and shaken at 100 rpm for 1 h at 75–95°C until isotropic microscopically. After microfiltration through a 0.22-μm Swinnex-GS filter assembly preheated to 75–95°C, ≈0.1 ml sample was taken for lipid analysis. To enter the crystallization sequence, stock solutions were divided and diluted as before (12) but at higher temperatures and then quenched to 4°, 23°, and 37°C giving CSIs of 1.2–2.7.

To monitor relative lipid compositions of the mother biles during crystallization and to prove that equilibration had occurred, duplicate portions of the concentrated (7.3 g/dL) TC-L-Ch and TCDC-L-Ch systems were microfiltered (37°C) as above at 0, 14–17, and 30 days and lipid compositions of the separated micellar phases were analyzed. Because of the possibility that repeated daily sampling of 5 μL to monitor crystallization might alter the composition of the mother biles artefactually, additional concentrated TC-L-Ch systems

spanning the same compositions were prepared and each was divided into two equal parts. One portion was allowed to crystallize with infrequent sampling (6–8 times), and the other was sampled every day for 30 days. After microfiltration, the lipid compositions of the separated mother biles in both TC systems were determined at 0, 15–17, and 30 days.

To study the effects of calcium concentration, we prepared stock MBS-L-Ch micellar biles (≈29 g/dL) with 5, 10, or 20 mM $CaCl_2$ at pH 7.0 and sufficient aqueous NaCl to maintain the ionic strength at 0.15 M. To induce supersaturation, the stock biles were diluted 4-fold with aqueous $CaCl_2$ plus NaCl which decreased the total lipid concentration ([TL]) to 7.3 g/dL and increased estimated CSIs from a mean of 0.96 ± 0.04 to 1.17 ± 0.06 (21). After incubation at 37°C and daily sampling for determination of crystal appearance times, crystal number was assayed by counting crystals in 5-μL samples for 5 days using a microscopic field of 1 cm^2 (× 200 magnification). In a parallel study with the MBS-L-Ch systems (37°C), 5-μL samples were removed for microscopic study every 2–3 days and the influences of 0, 10, and 20 mM $CaCl_2$ on the micellar phase boundary were assessed by lipid analysis of the microfiltered mother biles at 0 and 30 days (**Table 3**).

Quasi-elastic light-scattering spectroscopy (QLS)

To monitor particle sizes, QLS measurements of mean hydrodynamic radius $(\bar{R}_h)$ and polydispersity were performed on 1-mL samples of the initial stock biles and supersaturated biles after 4-fold dilution, respectively, at intervals between 0 and 168 h. Samples were maintained individually at 4°C, 20°C, and 37°C by means of a Peltier thermostatic block (8). To remove dust, each sample was filtered once through a Swinnex-GS 0.22 μm filter at the appropriate temperature (24). At thermodynamic equilibrium (≤ 30 days) as evidenced by stability in the crystallization sequences (see below), all precipitates were separated from the mother biles by centrifugation (100,000 *g*, 37°C for 8 h) or microfiltration (0.22 μm filter, 20°C) and QLS measurements were repeated on the isotropic phases. Where appropriate, multicomponent analysis (24) was used to confirm the presence and sizes of two or more discrete particle populations.

Detection times of solid cholesterol crystals and liquid crystals

After QLS, each model bile was subdivided into three samples and incubated without shaking at temperatures of 4°, 23° (R.T.), and 37°C. Crystallization times and pathways were determined by the method of Konikoff

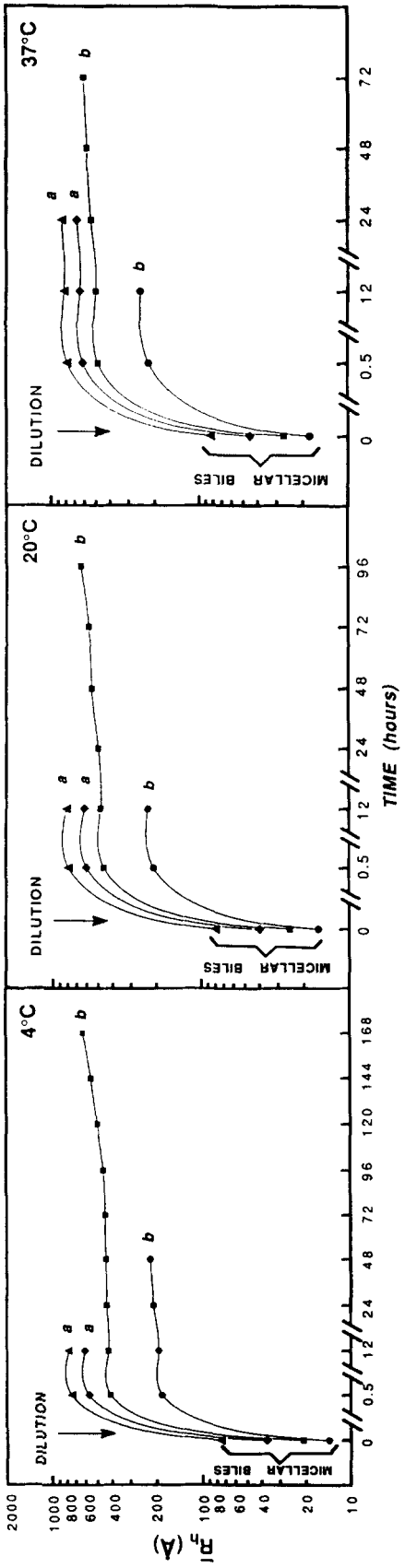

Fig. 1. Mean hydrodynamic radii ($\bar{R}_h$, in Ångstroms) of particles in model biles as functions of time before (0) and after 4-fold dilution of ≈29 g/dL micellar systems (Table 1) at 4°C, 20°C, and 37°C, respectively. Letter "a" on curves indicates that QLS was terminated because of excess turbidity due to nonbirefringent liquid crystals as verified by polarized light microscopy. Letter "b" on curves indicates the times when biles produced marked fluctuations in light scattering as evidenced later by microscopic evidence of solid crystals. Symbols (mean values) represent: ●–● for 0 < L/TC, L/TCDC and L/MBS < 0.2; ■–■ for 0.2 < L/TC, L/TCDC and L/MBS < 0.4; ◆–◆ 0.4 < L/TC, L/TCDC and L/MBS < 0.6; ▲–▲ for 0.6 < L/TC, L/TCDC and L/MBS < 1.0, respectively.

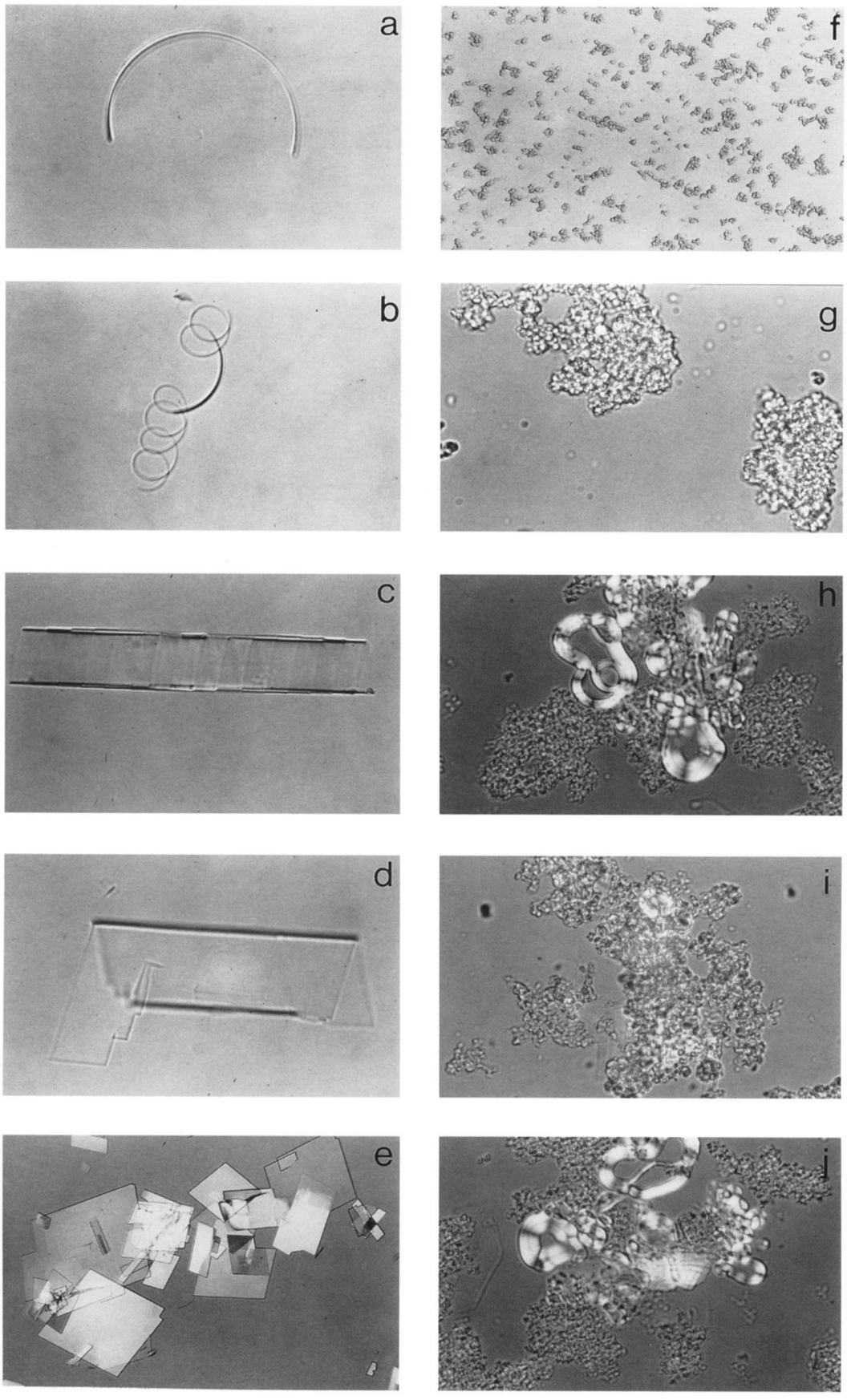

Fig. 2(a–j). Habits of solid and liquid crystals of Ch observed in this study by polarizing light microscopy: (a) arc-like crystal; (b) irregular right-handed helical crystal; (c) tubular crystal with helical stripes; (d) tube-like crystal fracturing at ends to produce plate-like ChM crystals; (e) typical ChM crystals, with 79.2° and 100.8° angles, and often a notched corner; (f) small non-birefringent liquid crystals (labeled "small"); (g) aggregated non-birefringent liquid crystals (labeled "aggregated"); (h) typical fused liquid crystals (labeled "fused") with Maltese-cross birefringence and focal conic textures; (i) ChM crystals emerging from an aggregated liquid crystal; and (j) same, from fused liquid crystals. All magnifications × 800.

et al. (12) with minor modifications. In brief, 5-μL samples were taken from the bottom third[4] of a 1-mL sample and placed immediately on a glass slide at ≈23°C. Initial observation by polarized light microscopy was without a cover slip and then with a cover slip using phase contrast optics (Photomicroscope III; Carl Zeiss Inc., Thornwood, NY). Crystallization sequences were examined at 2-h intervals for 12 h and then every day for 30 days with permanent documentation by 35 mm time-lapse photography. Processed films were used for measurement of different Ch crystal habits as well as identifying liquid crystalline textures. Pitch angles of helical crystals were measured by the methods of Chung et al. (13). Detection times were defined as the intervals from dilution to the earliest microscopic detection of noncompressible solid and compressible liquid crystals (× 400 magnification). Where denoted, detection times of ACh,[5] ChM, and liquid crystals (see subcategories below) were the times required for the earliest appearances of non-compressible arc-like crystals, plate-like parallelepiped crystals, and small compressible non-birefringent droplets, respectively.

Sucrose density gradient centrifugation

Linear (2 to 20%) sucrose density gradients were prepared in 13.2-mL nitrocellulose tubes (14, 25), and densities (d) were verified using marker beads (Pharmacia-LKB Biotechnology, S-751 82, Uppsala, Sweden). Ultracentrifugation of authentic ACh and ChM standards (19) resulted in bands of d 1.034 g/mL and d 1.048 g/mL, respectively, identical with literature values (15, 26). Liquid crystals and Ch crystals in the mother biles were concentrated by centrifugation, then layered on top of the gradients and centrifuged (20°C) in a SW41 Ti rotor (Beckman Instruments Inc., Fullerton, CA) at 201,000 *g* for 8 h (14, 25). Fractions were aspirated from top to bottom with an L-shaped Pasteur pipette and examined microscopically (14).

Lipid analysis

BS concentrations were assayed by the 3α-hydroxysteroid dehydrogenase method (27), L by an inorganic phosphorus procedure (28), and Ch enzymatically (29). Calculation of CSIs in model biles containing TC, MBS, and TCDC were based on the critical tables plus its appendix which incorporate correction factors for TUDC (21). Within experimental error, maximal Ch solubilities in the TC-L-Ch systems were identical to those published in the critical tables (21), and were remarkably close to present experimental values for the

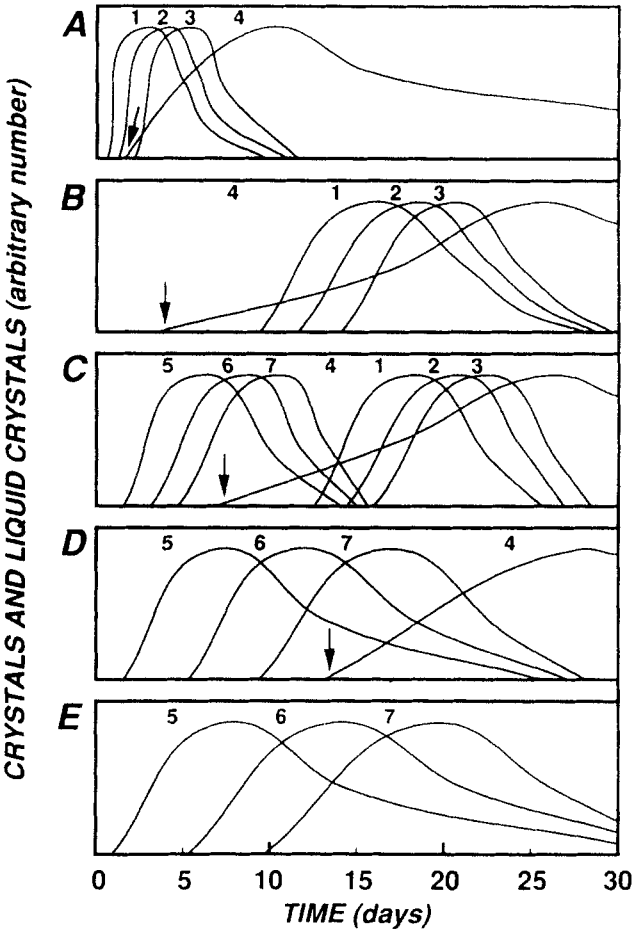

Fig. 3(a–e). Crystallization sequences subdivided into pathways **A, B, C, D,** and **E** based on the principal habits observed in the most concentrated (≈7.3 g/dL) MBS system at 37°C (0.15 M NaCl, pH 7.0). The vertical axes represent arbitrary numbers of crystals and liquid crystals per high power microscopic field, all normalized to the same maximum. Consecutive numbers represent (1) arc (most likely ACh), (2) helical, (3) tubular, and (4) plate-like ChM crystals, and (5) small, (6) aggregated, and (7) fused liquid crystals, respectively (for pictures and definitions, see Fig. 2). The detection times of ChM crystals (arrows on baseline) were retarded progressively between pathways **A** and **D;** ChM crystals did not appear in pathway **E.** Because of repeated sampling, relative number of ChM crystals and liquid crystals are decreased artifactually at later time points. When frequent sampling was not carried out, microscopic liquid crystals were invariably present at 30 days in pathways **C** → **E** but were absent from pathways **A** and **B.** When temperature, total lipid concentration, and BS hydrophobicity were decreased, the curves of ACh crystals (numbers 1 to 3) and ChM crystals (number 4) moved to the right, whereas those of liquid crystals (numbers 5 to 7) shifted to the left.

[4]In preliminary studies we found that sampling from this portion of the tubes produced highly quantifiable sequences. A comparison of sequences and detection times in samples from top, middle, and bottom of a series of tubes of typical pathophysiological compositions revealed slight time-dependent differences only. These (not displayed) were considered inconsequential for the purposes of the present study.

[5]Konikoff and colleagues (12) were circumspect in making a decision with respect to the earliest filamentous crystals in TC-rich dilute model bile. The crystals were apparently ACh crystals as revealed by their habits, suggestive synchrotron X-ray spacings, and appropriate density. Nevertheless, more refined studies have yet to be carried out to conclusively prove that ACh and not a new ChM polymorph precipitates from bile under these circumstances.

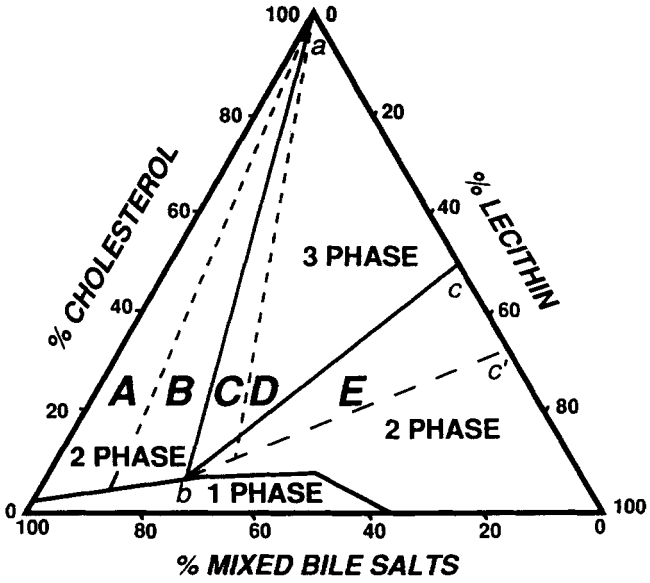

Fig. 4. Equilibrium phase diagram of MBS-L-Ch system (37°C, 0.15 M NaCl, pH 7.0, [TL] ≈7.3 g/dl) showing positions and configuration of crystallization regions (see pathways in Fig. 3). The components are expressed in moles percent. The micellar zone ("one-phase" at bottom) is enclosed by a solid curved line. The upper part of the triangle is divided by two dashed and two straight solid lines into regions **A** to **E** with different crystallization sequences (Fig. 3). The number of phases given represents the equilibrium state. They are ChM crystals and saturated micelles for crystallization regions **A** and **B**. ChM crystals, saturated micelles and liquid crystals with 1:1 Ch/L composition (point *c*) for regions **C** and **D** and liquid crystals of variable composition and saturated micelles for regions **E**. Note that in the case of regions **A, B, C, D** and **E,** metastable unilamellar vesicles (Fig. 1) with a Ch/L of 2:1 (8, 36) i.e., point *c'* may be present in biles at the initial time points of the study (see text for further details).

MBS-L-Ch and TCDC-L-Ch systems but not for the other BS (see results). Although during these long incubations rigorous measures such as N_2 purge and added NaN_3 were taken to avoid auto-oxidation of Ch (producing oxysterols) and spontaneous L hydrolysis (producing lysolecithin), their effectiveness was documented by HPLC (18) and thin-layer chromatography (19) of representative concentrated samples for all L mole fractions before and after 30 days incubation at 37°C. As evaluated by the two chromatographic methods, no lysolecithin was formed and no oxysterol peaks were detected.

RESULTS

QLS analysis of supersaturated model biles

Figure 1 shows the time dependence of $\bar{R}_h$ values before ([TL] of ≈29 g/dL) and after 4-fold dilution of TC-, TCDC-, and MBS-L-Ch systems at 4°C, 20°C, and 37°C, respectively. The stock Ch-saturated micellar biles (Table 1) contained a uniform population of particles with $\bar{R}_h$ (± SD) values of 16 ± 3Å (0 < L/TC, L/TCDC, and L/MBS < 0.2), 25 ± 4Å (0.2 < L/TC, L/TCDC, and L/MBS < 0.4), 42 ± 2Å (0.4 < L/TC, L/TCDC, and L/MBS < 0.6), and 82 ± 6Å (0.6 < L/TC, L/TCDC, and L/MBS < 1.0) at 20°C. As noted before (30) micellar $\bar{R}_h$ values of BS-L systems increase strongly with L content but only weakly with increases in temperature. By 0.5 h of dilution, the micellar biles had produced unilamellar vesicles as evidenced by an order of magnitude increases in $\bar{R}_h$ values (Fig. 1) and this was confirmed by vitreous ice electron microscopy (D. Q-H. Wang, D. Gantz, D. M. Small and M. C. Carey, unpublished observations). The post-dilution $\bar{R}_h$ values were 208 ± 11Å (0 < L/TC, L/TCDC, and L/MBS < 0.2), 464 ± 34Å (0.2 < L/TC, L/TCDC, and L/MBS < 0.4), 603 ± 16Å (0.4 < L/TC, L/TCDC, and L/MBS < 0.6), and 798 ± 16Å (0.6 < L/TC, L/TCDC, and L/MBS < 1.0) at 20°C increasing uniformly with L content. When the micelle plus vesicle biles entered the crystallization sequences (described below), reproducible autocorrelation functions could not be obtained because of large fluctuations in scattered light intensity (24). In systems that formed stable liquid crystals, (0.4 < L/TC, L/TCDC, and L/MBS < 1.0) QLS was terminated because of excess turbidity which was earliest at 4°C (Fig. 1).

Habits of crystals and textures of liquid crystals

Figure 2 (a–h) documents habits of solid Ch crystals and optical textures of liquid crystals. Arc-like crystals (Fig. 2a) were short curved rods. Sometimes longer filaments were found that varied in length from 10 to several hundred μm. Long arcs usually coiled into irregular helices or spirals (Fig. 2b). Over time these increased in length and number to form a population of right-handed regular helices. Initially, helices had small diameters and pitch angles of ≈56 ± 3° which decreased to ≈11 ± 2° (13). At later times, helices widened and fused to become ribbed cylindrical structures (Fig. 2c), whose length varied from 10 to several hundred μm (12, 13). Tubular crystals fractured frequently at their ends (Fig. 2d) to produce plate-like ChM crystals (Fig. 2e) with angles of 79.2° and 100.8°, and frequently a notched corner (31, 32). Figure 2f demonstrates the earliest appearing liquid crystals denoted as small, which were minimally sized, scattered, and non-birefringent. After a few days, small liquid crystals began to cluster (Fig. 2g) forming non-birefringent 1–5 μm particles, defined here as aggregated liquid crystals. At later time points, these fused into typical lamellar liquid crystals (Fig. 2h), which displayed characteristic focal conic textures and Maltese-cross birefringence (33, 34). The sizes

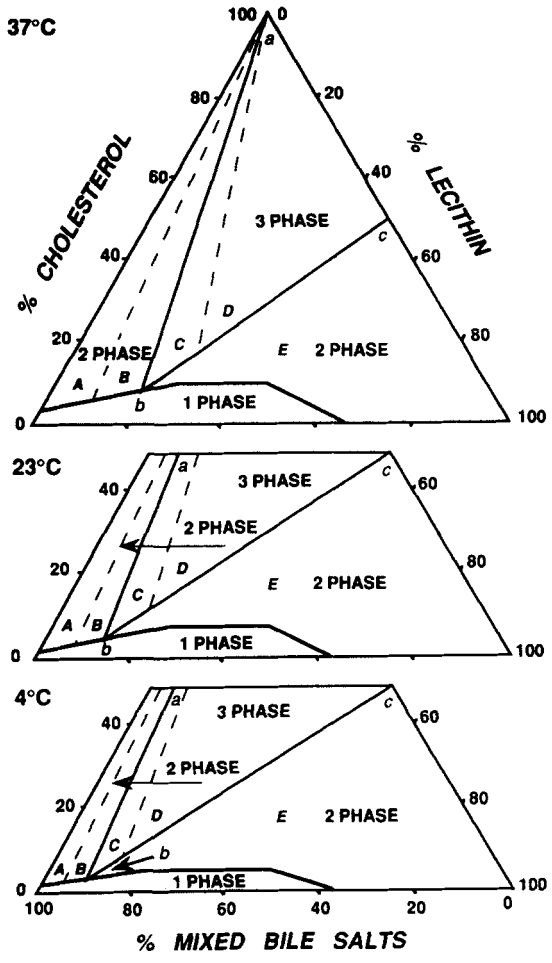

Fig. 5. Positions of crystallization regions **A–E** in the MBS-L-Ch system as functions of variations in temperature (4°C to 37°C). Other conditions are 0.15 M NaCl, pH 7.0, and [TL] ≈7.3 g/dL. All model bile systems exhibit the same physical states, at equilibrium, as in Fig. 4, but with decreases in temperature, crystallization pathways are shifted to the left, thereby generating a series of new condensed phase diagrams.

of fused liquid crystals varied considerably, but were usually greater than 0.5–1 μm.[6] Only aggregated and fused liquid crystals (Figs. 2i, 2j) developed irregular sharp edges with acute (≈82 ± 2°) or obtuse angles (≈95 ± 4°) and afterwards these remodeled into typical ChM crystals.

Crystallization pathways and time sequences

Figure 3A–E shows crystals and liquid crystals in arbitrary numbers as functions of time for stepwise increases in L mole fraction which defined pathways **A, B, C, D,** and **E** (sequences described below). Crystallization is shown for ~7.3 g/dL MBS-L-Ch systems in 0.15 M NaCl at 37°C. Arabic numerals 1–7 refer consecutively to curves of (1) arc, (2) helical, (3) tubular, (4) plate-like crystals, and (5) small, (6) aggregated, and (7) fused liquid crystals respectively (see Fig. 2). The position of each of these pathways is shown as crystallization regions on the condensed phase diagram for the MBS-L-Ch system at 37°C in **Fig. 4.**

Figure 3A depicts the crystallization sequence in region **A** (Fig. 4). The first precipitates were arc crystals, followed by helical and tubular crystals (as in Fig. 2a–c); ChM crystals (Fig. 2e) appeared after helical crystals were detected, and became predominent only when other crystals had disappeared. Some short arc crystals grew laterally to become flat ribbon-like crystals, or several long arc-crystals uncoiled in the middle or at one or both ends to grow into typical ChM crystals. At 4°C (not displayed) and in the higher [TL] systems, long bar-like crystals appeared, which grew into plate-like units. In dilute TC-L-Ch systems, and with high TC to L ratios, long filamentous crystals rather than arcs were observed, and they extended to several hundred μm (12). Only occasionally were filamentous crystals observed in other BS systems and they never appeared in TUDC-L-Ch systems. Furthermore, arc, helical, tubular, and ChM crystals were absent in dilute TUDC-L-Ch systems. Detection times of ACh and ChM crystals in pathway **A** (Fig. 3) became more prolonged in the rank order of systems containing TC < C < MBS < GC < TCDC < TDC < TUDC.

Figure 3B shows that in region **B** (Fig. 4) the crystallization pathway demonstrated plate-like ChM crystals initially, followed by the transient appearances of arc, helical, and tubular crystals at later time points. Tubular crystals uncoiled or fractured producing plate-like ChM crystals. It appeared that most ChM crystals in pathway **B** (Fig. 3) crystallized de novo from solution via a different route. Filamentous crystals (12–14) were rarely seen except with low [TL] and they were absent in TUDC-L-Ch systems. Crystal detection times in this region followed the rank order of biles containing TC < MBS < TCDC < TDC < GC < C < TUDC.

Figure 3C shows that in region **C** (Fig. 4) small liquid crystals as evidenced grossly by development of turbidity, were present at 2 days. Within a few days they aggregated and/or fused forming particles 1–5 μm in size (Fig. 2 f, g). Only large liquid crystals such as those shown in Fig. 2 i, j developed edges that transformed into semisolid crystals and then typical ChM plates. Fourteen to 16 days after ChM crystals became visible, the number of liquid crystals decreased and arc (occasionally filaments), helical, and tubular crystals ap-

[6]Because they were visible by optical microscopy, all liquid crystals observed must have been multilamellar vesicles of different sizes. The arbitrary dimensional division of these particles into small, aggregated, and fused has sequence significance for descriptive purposes only in this work and is not meant to imply differences in structure.

peared at similar times in all systems; but were slowest and infrequent in TUDC-L-Ch systems. After 2–3 days of coexisting with liquid crystals, ACh and other metastable crystals disappeared being replaced by ChM plates. Liquid crystal detection times were prolonged in the rank order of systems containing TC < GC < C < MBS < TUDC < TCDC < TDC.

Figure 3D shows that in region **D** (Fig. 4) crystallizing biles contained many small liquid crystals at 2 days that slowly aggregated and fused to form typical focal conics with Maltese-cross birefringence (33, 34). Generally most ChM crystals were observed in association with aggregated or fused liquid crystals and some free in solution. Arc, helical, and tubular crystals were never observed in this pathway. Detection times of both liquid crystals and ChM crystals were similar for all model biles except that solid crystals were much slower to appear in TUDC-L-Ch systems. In an apparent precursor–product relationship with increasing numbers of ChM crystals (Fig. 3D) liquid crystals decreased in number but were not eliminated by 20–27 days.

Figure 3E demonstrates that only liquid-crystals occurred in region **E** (Fig. 4). All model biles became turbid by 1 day, and small liquid crystals were detected microscopically. By 5 to 10 days, liquid crystals began to aggregate, fuse and at 12–13 days coalesced to form a macroscopic precipitate phase, but a transformation to ChM crystals did not occur. As predicted from theoretical phase equilibria considerations (35), myelin figures (33, 34) were observed occasionally in this pathway.

As Figure 4 shows, although liquid crystals must be present at equilibrium, i.e., end of crystallization, in pathways/regions **C, D,** and **E** (Figs. 3, 4) frequent sampling, especially from the bottom third of tubes (see footnote 4), depleted their numbers considerably so that they were difficult to detect in region **C** and sometimes in **D.** However, this was less of a problem in region **E** or at 4° and 23°C than at 37°C. Further, liquid crystals that apparently "nucleated" ChM crystals in these pathways were physically removed with solid crystals. It is also important to note that at the initiation of crystallization, the vesicle Ch to L ratio (Fig. 1) of systems falling into pathways C and D could be as high as 2:1 (8, 36). The latter ratio is suggested by the broad dashed line in the phase diagram through region **E** (Fig. 4) which intersects the Ch-L axis at *c'*. However, at equilibrium, the Ch/L ratio in liquid crystals is 1:1 (7) i.e., plotting at point *c*. This change in the phase boundary between metastable and equilibrated states facilitated an investigation of pathway **D** at CSIs between 2.1 (Table 2, Fig. 4) and 2.7 (see Methods). Another important issue is that considerable time-variations occurred within each crystallization pathway in that the sequences shown in Fig. 3 could occur faster or slower depending on whether the relative composition was in the left or right margins of the region (Fig. 4).

Density gradient centrifugation of crystallizing biles

For crystallizing TC-, TCDC-, or MBS-L-Ch systems plotting in regions **A** and **B** (Figs. 3, 4) density gradient centrifugation and microscopy at 2–3 days of crystallization yielded bands of arc crystals at a d 1.031 g/mL and plate-like ChM crystals at d 1.046 g/mL (14). With systems crystallizing with sequences of region **C,** (Figs. 3, 4) bands of arc crystals at a d 1.030 g/mL were found at 14–17 days together with plate-like ChM crystals at a d 1.045 g/mL and liquid crystals at a d 1.020 g/mL. Upon standing for 96 h (37°C), mixtures plotting in regions **A, B,** and **C** (Fig. 3, 4) revealed that arc crystals had transformed into helical, tubular, and plate-like crystals, consistent with hydration and subsequent mi-

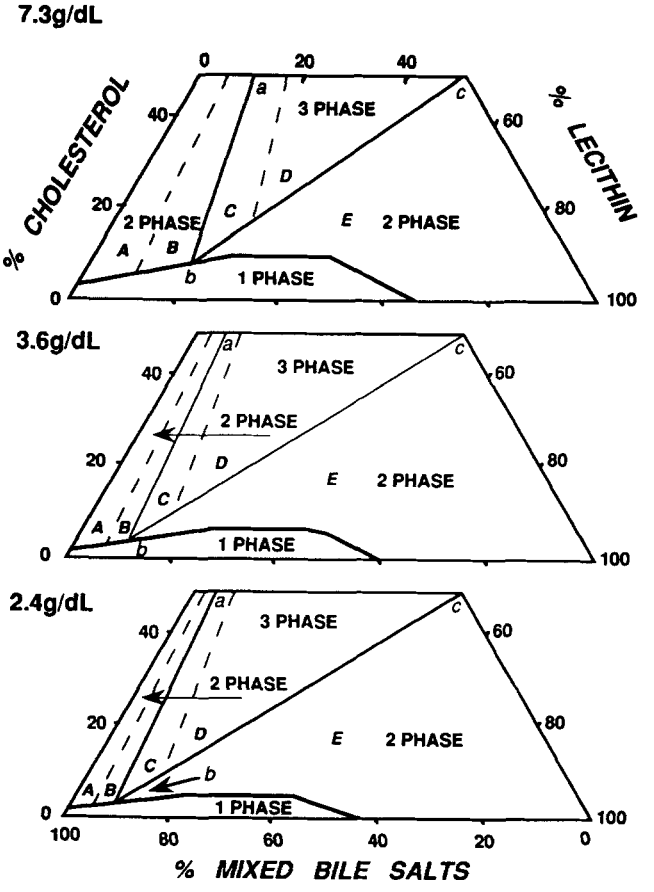

Fig. 6. Positions of crystallization regions **A–E** in the MBS-L-Ch system as [TL] was varied (≈2.4-7.3 g/dL). Other conditions are 37°C, 0.15 M NaCl, and pH 7.0. These systems exhibit the same physical states at equilibrium, as described for Fig. 5. With decreases in total lipid concentration, all crystallization pathways shifted to the left, thereby generating a series of new condensed phase diagrams.

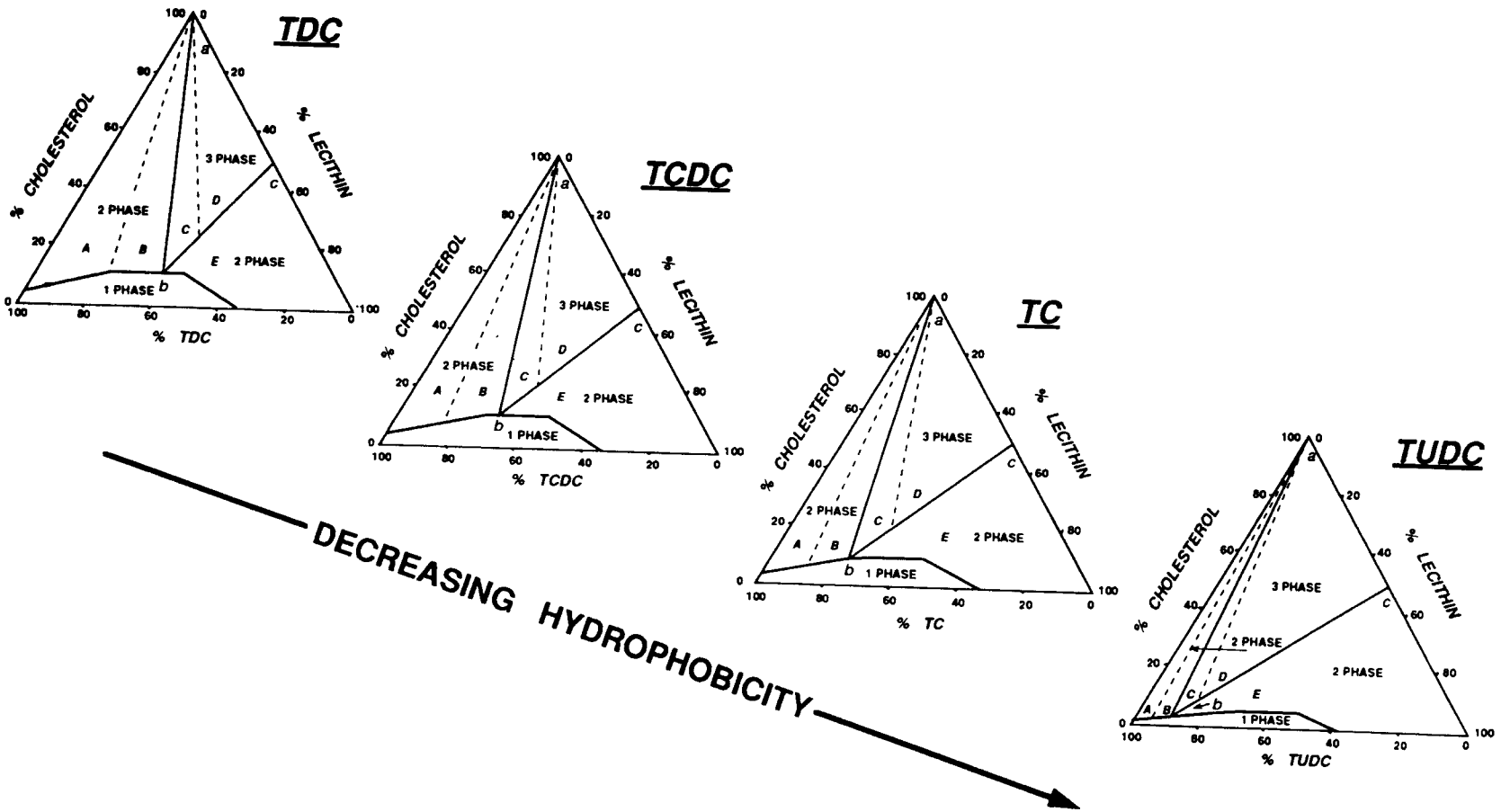

Fig. 7. Positions of crystallization regions **A–E** for decreasing BS hydrophobicity (TDC-, TCDC-, TC-, and TUDC-L-Ch systems) at [TL] of ≈7.3 g/dL. Other conditions are 37°C, 0.15 M NaCl, pH 7.0. These systems are in the same format as Fig. 4 and exhibit the same physical states at equilibrium as shown for Figs. 4–6. As the BS hydrophobicity decreased, so did the maximum micellar cholesterol solubility and crystallization pathways **A–E** moved to the left. Further details are given in the text.

gration in the centrifuge tube to a d of ChM (14). With crystallizing biles typifying sequences in region **D,** (Figs. 3, 4) density gradient centrifugation at 15–18 days yielded bands of plate-like ChM crystals (d 1.045 g/mL) and liquid crystals (d 1.021 g/mL). In contrast, density gradient centrifugation at 10–13 days of mixtures typifying the stable liquid crystals in region **E** yielded a single liquid crystalline band displaying focal conics (33, 34) at a d 1.022 g/ml and no ACh or ChM crystals.

General influence of physical chemical variables on crystallization

When temperature, [TL], and BS hydrophobicity were decreased, crystallization regions **A–E** (Fig. 4) shifted progressively to lower L contents. Moreover, all ACh (1, 2, and 3) and ChM (4) crystallization curves shifted to the right, i.e., became slower (Fig. 3) whereas liquid crystalline curves (5, 6, and 7) generally moved to the left, i.e., became faster.[7] In regions **A** and **B** (Fig. 4), ACh and ChM crystal detection times in all BS systems with [TL] = 7.3 g/dL were prolonged 1- to 2-fold at 23°C

[7]Detailed nucleation paths and phase equilibria data for the effects of individual bile salts (TUDC, TC, TCDC, TDC, GC, and C) at different temperatures (4°–37°C) and for variations in total lipid concentration (2.4–7.3 g/dL) are available upon written request from the corresponding author. However, the reader must temper the actual time sequences with caution, as they are not a stepped function across a region (Fig. 4) but are a continuum.

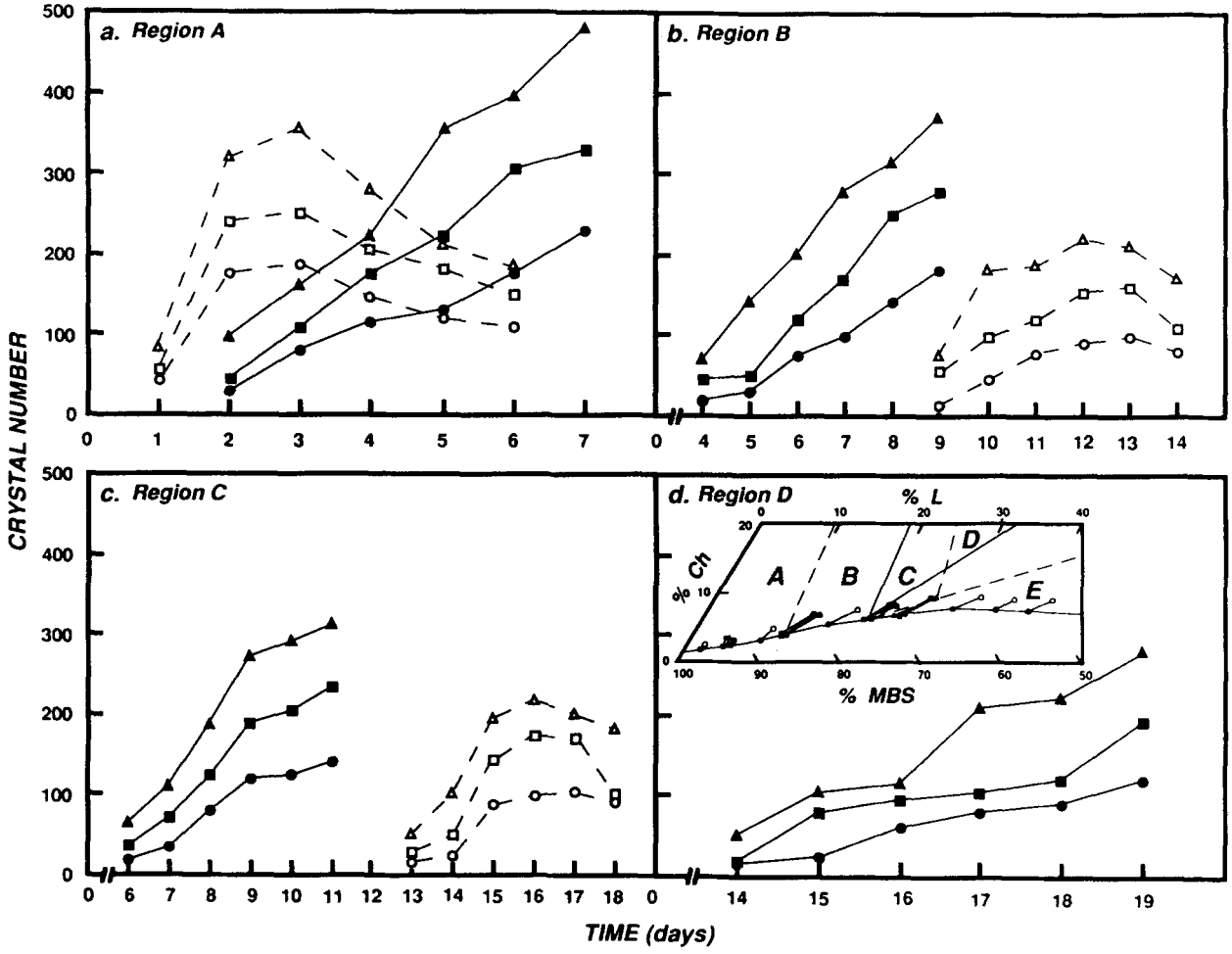

Fig. 8(a–d). Influence of calcium concentration on the numbers of ACh crystals (arc and other metastable crystals) and ChM crystals (plate-like crystals) per 5-μl bile samples. Open symbols represent numbers of ACh with increasing calcium concentration, ○–○ 5 mM; □–□ 10 mM; △–△ 20 mM calcium, respectively. Closed symbols represent ChM with increasing calcium concentration; ●–● 5 mM; ■–■ 10 mM; ▲–▲ 20 mM calcium, respectively. The inset in d shows the experimental condensed phase diagram and crystallization regions with 0, 10, and 20 mM added $CaCl_2$; data points (open symbols, no Ca^{2+}, with daily sampling, closed squares and circles, with Ca^{2+}, every 2–3 day sampling) represent changes in composition of micellar biles at 30 days compared to the systems at time 0. Panels a to d correspond to crystallization pathways in regions **A** to **D** as denoted by the inset in panel d. Dashed curve in **E** of inset shows the 2:1 Ch/L ratio of supersaturated vesicles and explains how pathway **D** enters detectable compositions when CSI is ≈1.2 (Table 3). Other conditions were MBS, 37°C, pH 7.0, and [TL], initial TL ≈7.3 g/dL and final [TL] (micellar) ≈6.1–6.3 g/dL (see Table 3). Note that for clarity, liquid crystal numbers are omitted from regions **C** and **D.**

TABLE 4. Analytical lipid compostions of crystallizing biles before, during and after 30 day incubation

	Day 0					14-17 Days					30 Days				
Number	Mole%Ch	Mole%L	Mole%BS	[TL] (g/dl)	CSI	Mole%Ch	Mole%L	Mole%BS	[TL] (g/dl)	CSI	Mole%Ch	Mole%L	Mole%BS	[TL] (g/dl)	CSI
A. TC-L-Ch (n = 2–4)[a]															
1	2.71 ± 0.02	1.95 ± 0.00	95.35 ± 0.02	7.44 ± 0.04	1.26 ± 0.01	2.42 ± 0.11	1.58 ± 0.11	96.00 ± 0.00	7.10 ± 0.06	1.14 ± 0.06	1.91 ± 0.17	1.46 ± 0.18	96.65 ± 0.35	6.35 ± 0.15	0.98 ± 0.00
2	3.53 ± 0.01	4.82 ± 0.00	91.65 ± 0.01	7.38 ± 0.01	1.27 ± 0.01	2.94 ± 0.06	4.28 ± 0.61	92.78 ± 0.66	7.27 ± 0.07	1.10 ± 0.04	2.54 ± 0.12	4.35 ± 0.16	93.12 ± 0.28	6.05 ± 0.07	0.98 ± 0.01
3	4.76 ± 0.03	9.53 ± 0.01	85.72 ± 0.02	7.43 ± 0.04	1.23 ± 0.01	4.03 ± 0.25	8.16 ± 0.30	87.82 ± 0.55	7.10 ± 0.06	1.15 ± 0.02	3.19 ± 0.09	7.61 ± 0.71	89.21 ± 0.81	6.21 ± 0.16	0.99 ± 0.01
4	6.35 ± 0.02	14.05 ± 0.00	79.61 ± 0.02	7.42 ± 0.01	1.27 ± 0.00	4.86 ± 0.15	12.47 ± 0.11	82.68 ± 0.25	7.02 ± 0.05	1.08 ± 0.03	3.99 ± 0.16	11.21 ± 0.25	84.81 ± 0.41	6.15 ± 0.06	0.98 ± 0.00
5	7.22 ± 0.13	18.56 ± 0.02	74.23 ± 0.11	7.34 ± 0.06	1.19 ± 0.02	6.02 ± 0.57	16.53 ± 1.06	77.45 ± 1.63	7.05 ± 0.23	1.07 ± 0.04	5.11 ± 0.06	16.19 ± 0.35	78.71 ± 0.41	6.20 ± 0.06	0.97 ± 0.01
6	8.02 ± 0.39	23.00 ± 0.10	68.99 ± 0.30	7.25 ± 0.04	1.15 ± 0.06	7.26 ± 0.08	20.58 ± 0.54	72.16 ± 0.62	6.93 ± 0.00	1.14 ± 0.02	6.10 ± 0.14	20.16 ± 0.51	73.74 ± 0.65	6.02 ± 0.03	0.99 ± 0.00
7	8.87 ± 0.52	27.34 ± 0.16	63.80 ± 0.36	7.35 ± 0.03	1.16 ± 0.07	8.33 ± 0.47	25.33 ± 0.82	66.34 ± 1.29	7.23 ± 0.04	1.14 ± 0.04	6.95 ± 0.08	24.86 ± 0.49	68.20 ± 0.57	6.00 ± 0.01	1.00 ± 0.01
8	9.53 ± 0.07	31.67 ± 0.02	58.81 ± 0.05	7.46 ± 0.06	1.21 ± 0.01	8.77 ± 0.19	31.11 ± 0.34	60.13 ± 0.15	7.11 ± 0.11	1.12 ± 0.03	7.47 ± 0.16	30.43 ± 1.05	62.11 ± 0.90	6.19 ± 0.03	0.99 ± 0.02
9	9.54 ± 0.04	36.19 ± 0.01	54.27 ± 0.01	7.48 ± 0.04	1.22 ± 0.01	9.17 ± 0.08	34.97 ± 0.74	55.86 ± 0.65	7.19 ± 0.11	1.17 ± 0.01	7.58 ± 0.01	35.04 ± 0.54	57.39 ± 0.55	6.24 ± 0.02	0.99 ± 0.00
10	9.16 ± 0.01	40.88 ± 0.01	49.97 ± 0.01	7.49 ± 0.02	1.20 ± 0.00	8.47 ± 0.03	40.73 ± 0.37	50.81 ± 0.35	7.27 ± 0.05	1.12 ± 0.01	7.52 ± 0.16	38.04 ± 3.06	54.45 ± 2.90	6.38 ± 0.08	1.00 ± 0.01
11	8.91 ± 0.01	45.55 ± 0.01	45.55 ± 0.01	7.47 ± 0.04	1.15 ± 0.00	8.25 ± 0.50	44.24 ± 1.67	47.52 ± 1.17	7.22 ± 0.08	1.09 ± 0.07	7.43 ± 0.01	44.80 ± 0.19	47.78 ± 0.18	6.51 ± 0.08	1.00 ± 0.00
Mean ± SD				7.41 ± 0.08	1.21 ± 0.05				7.13 ± 0.13	1.12 ± 0.04				6.21 ± 0.16	0.99 ± 0.01
B. TCDC-L-Ch (n = 1)															
1	2.69	1.95	95.36	7.38	1.25	2.22	1.29	96.49	7.14	1.17	1.78	1.50	96.72	6.45	0.97
2	3.56	4.82	91.62	7.31	1.28	2.83	4.37	92.80	7.32	1.10	2.45	3.83	93.72	6.00	0.99
3	4.88	9.51	85.61	7.33	1.26	3.91	8.25	87.84	7.06	1.15	3.31	7.34	89.35	6.32	0.99
4	6.40	14.04	79.56	7.34	1.28	5.20	12.30	82.50	6.98	1.16	4.20	12.24	83.56	6.11	0.96
5	7.55	18.49	73.96	7.29	1.24	6.34	16.66	77.00	7.21	1.13	5.12	16.26	78.62	6.24	0.97
6	8.59	22.85	68.56	7.39	1.23	7.25	20.55	72.20	6.93	1.13	6.02	20.14	73.84	6.04	0.99
7	9.20	27.24	63.56	7.41	1.20	8.35	24.64	67.01	7.25	1.15	7.03	24.97	68.00	6.00	1.00
8	9.61	31.64	58.75	7.43	1.22	9.00	30.11	60.89	7.19	1.15	7.52	30.00	62.48	6.17	0.99
9	9.57	36.17	54.26	7.38	1.23	8.25	34.75	57.00	7.26	1.05	7.61	34.67	57.72	6.25	1.00
10	9.14	40.89	49.97	7.42	1.20	8.74	40.06	51.20	7.30	1.15	7.50	40.19	52.31	6.43	1.00
11	8.89	45.56	45.56	7.43	1.15	8.58	43.55	47.87	7.28	1.13	7.45	44.97	47.58	6.56	1.00
Mean ± SD				7.37 ± 0.05	1.23 ± 0.04				7.17 ± 0.13	1.13 ± 0.03				6.23 ± 0.19	0.99 ± 0.01

Abbreviations as in Table 1. Other conditions were 0.15 M NaCl, pH = 7.0, T = 37°C.

[a]All except two TC-L-Ch systems were sampled frequently during incubation to monitor crystallization sequences.

and 2- to 4-fold at 4°C compared to 37°C. In regions **C** and **D,** they were prolonged 0.3- to 1-fold at 23°C and 1- to 2-fold at 4°C compared to 37°C. In region **C** detection times of liquid crystals were shortened 0.5- to 2-fold at 23°C and 1- to 3-fold at 4°C compared to 37°C whereas in region **D,** they were prolonged by similar factors at 23°C and 4°C compared to 37°C. However, in region **E,** liquid crystal detection times were similar for all model bile systems and independent of temperature. When [TL] was decreased from 7.3 to 2.4 g/dL, detection times of ACh and ChM crystals in regions **A, B, C,** and **D** at 37°C (Fig. 4) were extended 1.5- to 2-fold, 1.2- to 1.5-fold, and 0.7- to 1-fold, respectively. Concomitantly, liquid crystal detection times in regions **C,** and **D** (Fig. 4) were shortened 1- to 1.5-fold, and 1- to 2-fold, respectively, but were similar for all model biles in region **E.** When BS hydrophobicity (37) was decreased (from TDC to TUDC), ACh and ChM crystal detection times at 37°C were extended 2.5 to 3.5-fold, 2.3- to 3.2-fold, 1.3- to 2.5-fold, and 0.8-fold, in pathways **A–D**

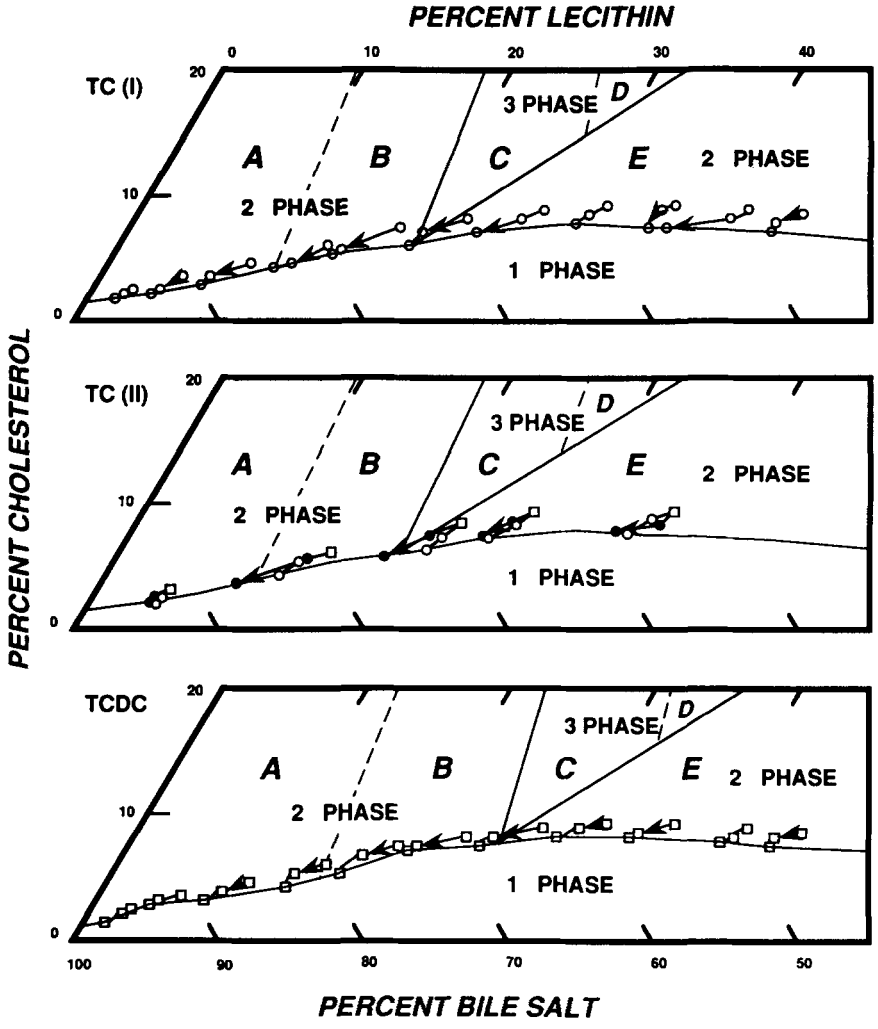

Fig. 9. Truncated phase diagrams with arrows connecting data points showing initial, intermediate, and final relative lipid compositions during crystallization for 30 days. The direction of the arrows shows that in general L/BS ratio decreases as the excess Ch precipitates. The lower left points demarcate the saturated micellar zone. In TC(I)-L-Ch, and TCDC-L-Ch systems the samples were observed microscopically at daily intervals. In the TC(II)-L-Ch system, daily samplings for microscopic observations were made in one set (closed symbols) but not in the other (open symbols). Right uppermost symbol of each cluster indicates day 0, middle symbol 14–17 days, and left lowest symbol 30 days of crystallization. Mean total lipid concentration of initial mixtures was ≈7.3 g/dL and at equilibrium for saturated micelles was ≈6.2–6.3 g/dL. In many cases, crystallization path boundaries are crossed explaining in part the crystallization sequences in Fig. 3. The fact that in TC(II) systems the changes in L/BS ratio in region **A** are not marked (in contrast to TC(I)) is consistent with absence of liquid crystals and persistence of unilamellar vesicles in this region (see also Fig. 8 d inset). Other conditions were 37°C, 0.15 M NaCl, pH 7.0, for further description see text.

([TL] ≈ 7.3 g/dL) respectively. However, by decreasing BS hydrophobicity, liquid crystal detection times in regions **C** and **D** were shortened 1- to 1.3-fold, and 1- to 1.5-fold, but were similar in region **E** for all BS. When L/(BS + L) ratio, [TL], and temperature were held constant, the detection times of ChM crystals were accelerated in the following rank order, TDC > TCDC > C ≥ TC ≈ MBS ≥ GC > TUDC for BS systems. Phase boundaries *ab* and *bc* (Fig. 4) are straight lines in all phase diagrams and all crystallization pathways are dependent on the position of point *b* as further shown below.

Influence of temperature on crystallization pathways

Because all crystallization pathways were followed to true equilibrium (e.g., Fig. 4) we display in **Fig. 5** the positions of the crystallization pathways as well as phase diagrams for the MBS-L-Ch system (7.3 g/dL, 0.15 M NaCl, pH 7.0) as functions of variations in temperature (4°–37°C). The 37°C diagram is the same as Fig. 4 where solid lines denote experimentally determined equilibrium phase boundaries and two dashed lines extending from the Ch apex further divide these into crystallization regions **A–E.** With decreases in temperature, all physical states and crystallization pathways are shifted to the left, i.e., to lower L contents, and concomitantly the micellar zone becomes progressively smaller. It is apparent that as the left two-phase zone became smaller (Fig. 5), the right two-phase area, (region **E**) where stable liquid crystals form, separates the central three-phase area from the micellar zone for typical pathophysiological compositions.

Influence of total lipid concentration on crystallization pathways

Figure 6 displays on truncated phase diagrams the crystallization pathways of MBS-L-Ch systems for variations in [TL] (2.4–7.3 g/dL) at 37°C (0.15 M NaCl, pH 7.0). These systems exhibit the same physical states and crystallization regions (**A** to **E**) as described in Figs. 4 and 5. It is clear however, that lowering [TL] had the same effect as lowering temperature (Fig. 5). As previously defined for the TC-L-Ch system (7), the micellar zone became smaller as [TL] decreased and contraction

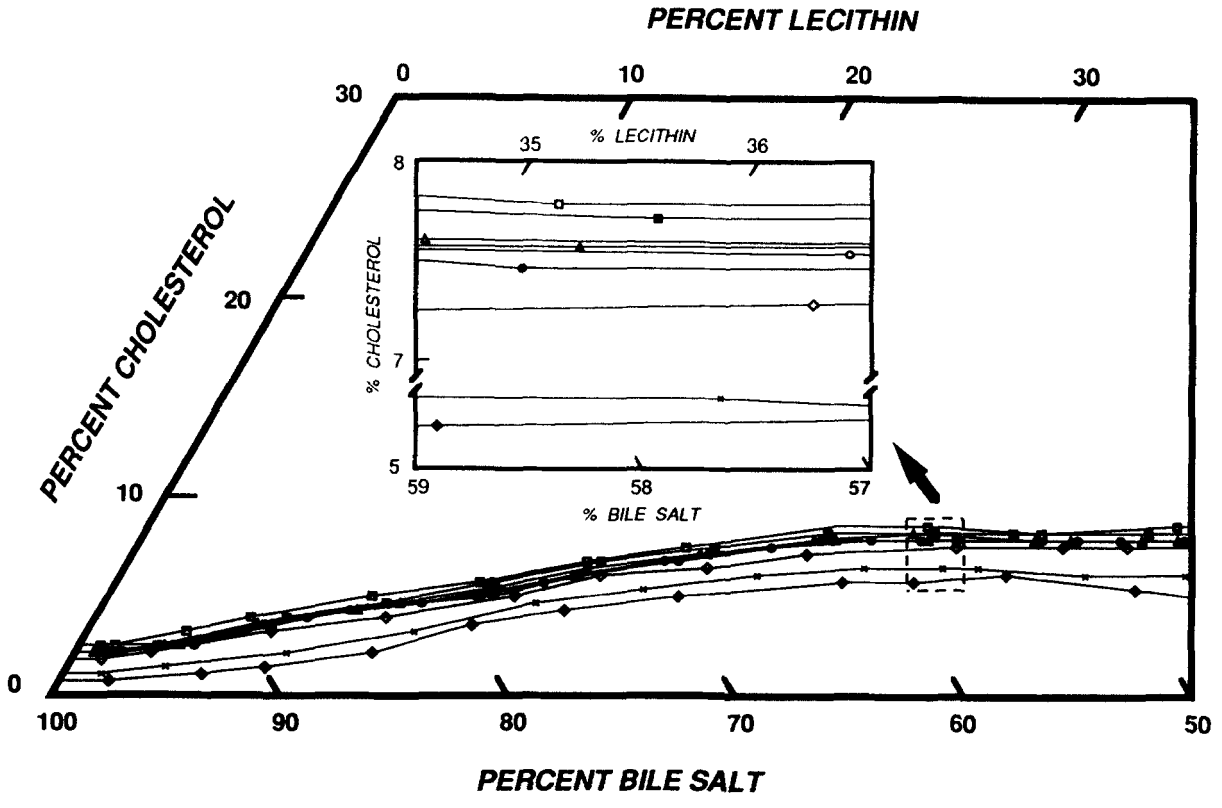

Fig. 10. Fragment of a triangular coordinate plot of equilibrium Ch solubilities in micellar BS-L-Ch systems (37°C) all at ≈6.0–6.2 g/dl and two sets (TC-, TUDC-L-Ch), derived from the critical tables (21) where the calculation was carried out for 10 g/dl in the case of TUDC-L-Ch systems. The inset indicates an enlarged portion of the equilibrium Ch solubilities between 57 and 59 moles % BS. The symbols in the inset and main figure from top to bottom are □, TDC-L-Ch; ■, C-L-Ch; △, TCDC-L-Ch; ▲, TC-L-Ch; (experimental), ○ TC-L-Ch (critical tables (21)), ●, MBS-L-Ch; ◇, GC-L-Ch; and x, TUDC-L-Ch (appendix plus critical tables (21)), and ◆, TUDC-L-Ch (experimental). Capacities of different BS to solubilize Ch is maintained with increases in L and for constant [TL] decreases in the rank order, TDC > C > TCDC ≥ TC ≈MBS > GC > TUDC.

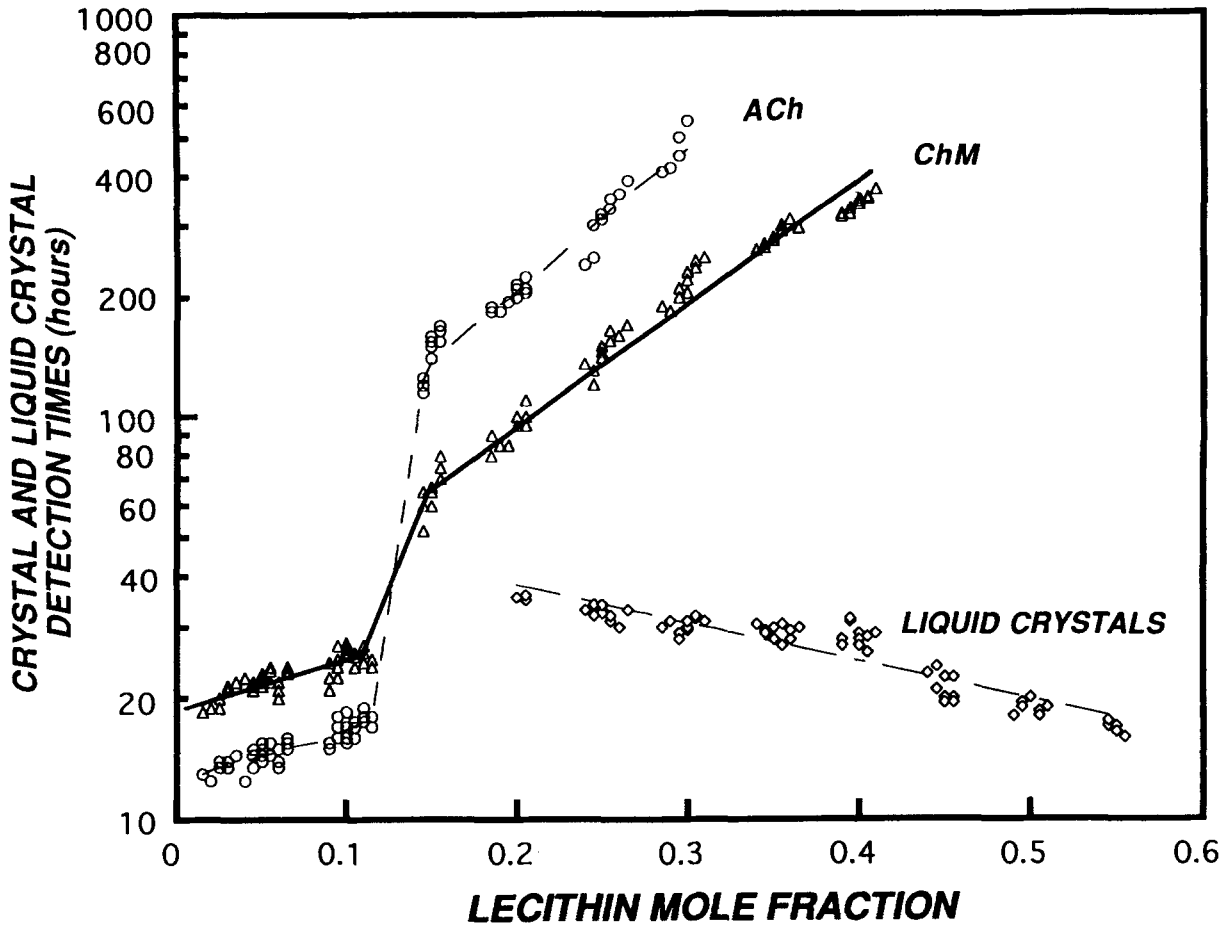

Fig. 11. Ch crystal and liquid crystal detection times as functions of L mole fraction (L/(BS + L) molar ratio) in combined TC-L-Ch, TCDC-L-Ch, and MBS-L-Ch systems which had similar crystallization and phase behavior (37°C, 0.15 M NaCl, pH 7.0, [TL] 7.4 g/dl, CSI 1.2 ± 0.1). At lowest L fractions, ACh crystal detection is earlier than that of ChM crystals. Between molar ratios of 0.13 and 0.20, ACh detection times lag behind those of ChM crystals. As L mole fraction is increased further, liquid crystals appear first, followed by ChM crystals, then ACh crystals and, with increasing L content, they diverge. Between L mole fractions of 0.30 and 0.42, liquid crystals are detected before ChM crystals and no ACh crystals appear. At lecithin mole fractions greater than 0.42, liquid crystals only appear. Symbol ○ represents ACh crystals, △ ChM crystals, and ◇ liquid crystals.

of the left two-phase zone occurred. Concomitantly, the right two-phase zone (region **E**) extended between the micellar zone and the central three-phase zone and overlapped pathophysiological compositions (Fig. 6), especially in the most dilute model bile.

Influence of bile salt hydrophobicity on crystallization pathways

In similar format, **Figure 7** displays the crystallization pathways as functions of BS hydrophobicity using the taurine conjugates of the common BS (37°C, 0.15 M NaCl, pH 7.0, [TL] ≈7.3 g/dL). When BS hydrophobicity (37) was decreased, all 2- and 3-phase zones and crystallization regions shifted progressively to the left and the micellar zone became contracted (38, 39). In the case of the MBS-L-Ch system (Fig. 4), the micellar zone and phase boundary *ab* were similar to that of the TC-L-Ch system, whereas in the GC-L-Ch system phase boundary *ab* was shifted slightly to the left and in the C-L-Ch system to the right (data not displayed). As point *"b"* moved to the left with decreasing BS hydrophobicity, region **E** extended to the left and overlapped pathophysiological compositions as exemplified in the TUDC-L-Ch system (Fig. 7). As shown in earlier work (39) this occurs also with a range of other very hydrophilic BS systems. On the assumption of additivity, this shift would be more dramatic if a hydrophilic BS-L-Ch system was dilute as well as cold (see Figs. 5, 6).

Influence of calcium on cholesterol crystallization pathways

Figure 8 (a–d) represents ACh and ChM crystal number for MBS-L-Ch compositions that plotted in crystallization regions **A, B, C, D,** (Fig. 4, Fig. 8d inset).

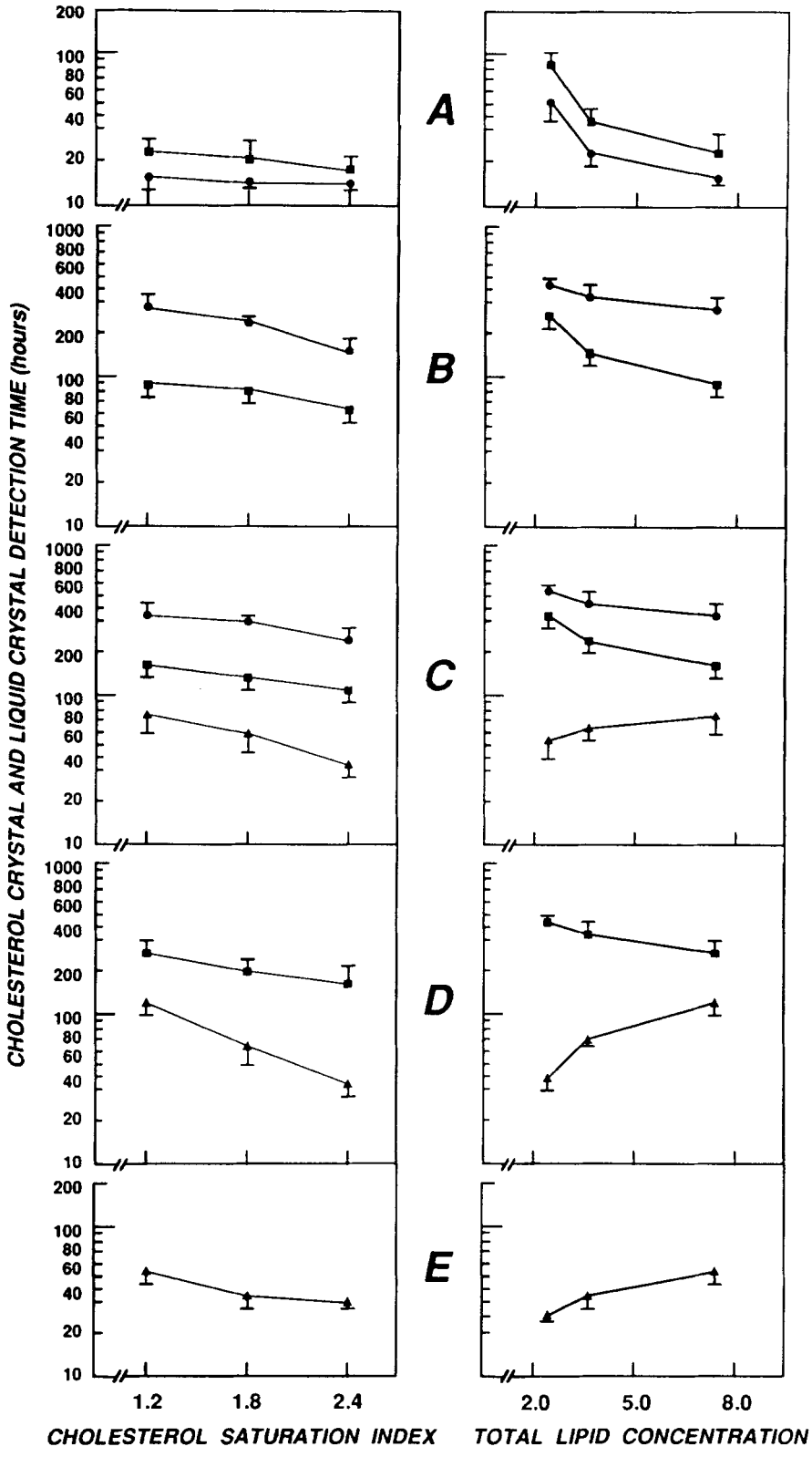

Fig. 12. Left panels: Summary data for TC-, TCDC-, and MBS-L-Ch systems (37°C, 0.15 M NaCl, pH 7.0) showing influence of CSI on Ch crystal and liquid crystal detection times for regions **A–E** (Fig. 3, 4) at constant [TL] of 7.3 g/dL (mean ± SD). The higher the CSI values, the shorter ACh, ChM, and liquid crystal detection times. Right panels: summary data showing influence of [TL] on Ch crystal and liquid crystal detection times for region **A–E** (Fig. 3, 4). As displayed by the ordinate, with 4- to 12-fold dilution, CSI values increased from 1.2 ± 0.0, to 1.4 ± 0.1, to 1.6 ± 0.0, and whereas this led to progressively longer ACh and ChM crystal detection times, it shortened liquid crystal detection times. In both panels, symbols ●–● represent ACh; ■–■ ChM; and ▲–▲ liquid crystals, respectively.

Compared to control biles without calcium (Fig. 3), Ch crystallization in MBS-L-Ch biles with 5, 10, or 20 mM added $CaCl_2$ did not display any alteration in solid crystal or liquid crystal detection times or crystallization pathways (Fig. 8 d inset). Nonetheless, Fig. 8 a–d shows that the numbers of solid Ch crystals were significantly greater in all model biles and increased stepwise in proportion to $CaCl_2$ concentration ($P < 0.001$). Fig. 8 a shows that in region **A** (Fig. 8 d inset), ACh crystals appeared at 1 day, reached a peak at 3 days, and gradually decreased in number, whereas the number of ChM crystals that appeared on day 2 progressively increased, suggesting a precursor–product relationship with ACh (14). Figure 8 b displays that in region **B** (Fig. 8 d inset) ChM crystals appeared at day 4 followed by ACh crystals on day 9, and no precursor–product relationship was apparent. Figure 8 c depicts the sequences of solid crystallization in region **C** (for clarity, liquid crystals are omitted). Although solid crystal appearance times were delayed 2–4 days, the behavior was similar to region **B** with ACh appearing after ChM. Figure 8 d illustrates that in region **D,** ChM crystals did not appear until 14 days (data for liquid crystals are omitted) and no ACh crystals were observed. Table 3 summarizes analytic lipid compositions of these MBS-L-Ch systems with 0, 10, and 20 mM added Ca^{2+} before and after the 30-day incubation. At time 0, [TL] was 7.0–7.5 g/dl with CSI of 1.2, whereas at 30 days, [TL] (micellar) was 6.1–6.4 g/dl and CSI was 1.0. As displayed by the inset phase diagram (Fig. 8 d), the relative lipid compositions of the MBS-L-Ch micellar phase with 10 (closed squares) and 20 mM (closed circles) $CaCl_2$ after 30 days equilibration were not appreciably different from 0 mM $CaCl_2$ (open and closed circles) and all final compositions plotted on the same micellar phase boundary (Fig. 8 d inset, left lower data points).

Changes in lipid compositions of mother biles during crystallization

Figure 8 d (inset) provides a glimpse of the fact that in the case of the calcium study the relative L/BS compositions of the mother biles changed during incubation for 30 days. This occurred irrespective of whether the tubes were sampled daily (0 mM Ca^{2+}) or every 2–3 days (10 mM and 20 mM Ca^{2+}). It is clear that all compositions shifted appreciably to lower L contents except in region **A.** This was addressed more formally in TC(I)- and TCDC-L-Ch systems (37°C, 0.15 M NaCl, pH 7.0) that were separated and analyzed at three time points during crystallization in addition to being sampled to monitor crystallization. Two identical TC(II)-L-Ch systems were also studied: in one crystallization was monitored every day and in the other the systems were sampled 6–8 times. This allowed us to check whether frequent sampling altered relative compositions artefactually at equilibrium (see Methods). As summarized in **Table 4,** initial biles had a mean [TL] of 7.4 g/dL and CSI of 1.2. By 14–17 days, [TL] (micellar) was 7.1–7.2 g/dL and CSI was 1.1, and by 30 days [TL] (micellar) was 6.2 g/dL and CSI was 0.99 indicating that equilibration had occurred. **Figure 9** illustrates, on truncated triangular coordinates, relative lipid compositions of initial, intermediate, and final mother biles for TC(I)-L-Ch (frequent sampling), TC(II)-L-Ch (frequent and infrequent sampling), and TCDC-L-Ch systems (frequent sampling) before, during, and after 30 days incubation. These results indicate that during Ch crystallization, relative compositions of crystallizing biles do not follow lines of constant L/BS ratio, but exhibit a progressive decrease in L mole fraction. This change was invariably greater with more frequent sampling than without, especially in region **A.** In many cases the change in L/BS ratio induces a traversal from one crystallization region to a neighboring one of lower L content (Fig. 9). It is apparent (Fig. 9) that the altered L/BS ratios are not an artefact of frequent sampling as TC(II) shows similar changes in composition in the absence as well as in the presence of frequent sampling. In region **A** there is a shift in L/BS ratio with daily sampling (TC(I)-TCDC) but not in the TC(II) study nor with added Ca^{2+} (Fig. 8 d). This suggests that only unilamellar vesicles and perhaps micelles were the crystallizing particles in pathway **A** (Fig. 3) as both of these particles would have passed through the microfilters. Because liquid crystals would be retained during microfiltration, it is apparent that L-containing multilamellar vesicles were retained in the other regions (Fig. 8 d inset, Fig. 9) in agreement with microscopic observations (see above). As L/BS ratio also shifted strongly in region **B** (Fig. 8 d) and where multilamellar vesicles are not expected (Fig. 4), it is likely that small metastable liquid crystals were present in this pathway although not microscopically visible.

Particle sizes in micellar biles at termination of crystallization

QLS analysis (20°C) of the microfiltered biles after 30 days incubation revealed micelles with mean $\bar{R}_h \pm$ SD values of 16 ± 3 Å (0 < L/TC, L/TCDC and L/MBS < 0.2), 25 ± 5 Å (0.2 < L/TC, L/TCDC and L/MBS < 0.4), and micelles coexisting with traces (< 0.1%) of unilamellar vesicles, giving $\bar{R}_h$ values of 39 ± 7 Å and 550 ± 43 Å (0.4 < L/TC, L/TCDC and L/MBS < 0.6), 79 ± 9 Å and 670 ± 64 Å (0.6 < L/TC, L/TCDC and L/MBS < 1.0). $\bar{R}_h$ values of both micelles and vesicles in each group increased as L/BS ratios increased and these values were either identical to or showed no appreciable differ-

ences from the $\bar{R}_h$ values of the stock (≈29 g/dL) micellar biles before dilution (see earlier results). This indicated the near lack of dependence of $\bar{R}_h$ values on [TL] under these conditions (30).

Cholesterol solubilities in equilibrated micellar biles

Figure 10 shows that at termination of crystallization, micellar Ch solubilities decreased in the rank order of systems containing TDC > C > TCDC ≥ TC ≈MBS > GC > TUDC. It is notable that Ch solubility in TC-L-Ch systems was essentially identical to the critical tables (21), and experimentally close to values for MBS-L-Ch and TCDC-L-Ch systems, indicating that TC, TCDC, and physiological MBS systems are highly similar (Fig. 10, inset). Furthermore, we confirmed that over the entire range of BS/L ratios, micellar Ch solubilities are significantly reduced in TUDC-L-Ch system (21) compared with TC- or MBS-L-Ch systems, and Ch solubility in the more dilute micellar lipid concentration of TUDC-L-Ch systems (37°C, 0.15 M NaCl, pH 7.0) was appropriately less than that 10 g/dL used in the critical tables (21) with adjustment for the correction factor in its appendix, (Fig. 10, inset). Figure 10 also shows that for C congeners, TC-containing systems solubilize less Ch than unconjugated C and more so than GC-containing systems.

Influence of lecithin mole fraction on crystal and liquid crystal detection times

Figure 11 summarizes, on a semilogarithmic scale, detection times of crystal and liquid crystals in the combined TC-, TCDC- plus MBS-L-Ch systems (7.3 g/dL, 37°C, 0.15 M NaCl, pH 7.0) all of which had similar crystallization behavior and Ch solubilities (Fig. 10). As the L mole fraction was increased, ACh crystals were detected rapidly and preceded ChM crystals by ≈10 h. Between an L mole fraction of 0.15 and 0.20, detection times of ACh crystals intersected the curve of ChM crystals at an L fraction of ≈0.13. At an L mole fraction between 0.20 and 0.30, liquid crystals appeared for the first time, followed by ChM crystals and subsequently ACh crystals. With further increases in L mole fraction, detection times of solid and liquid crystal diverged. Between L mole fractions of 0.30 and 0.40, liquid crystals preceded ChM crystals, but ACh crystals were absent. At L mole fractions above 0.40, detection times of liquid crystals became increasingly shortened but no solid crystals ever appeared.

Influences of CSI and total lipid concentration on detection times

Figure 12 (left panel) summarizes, on a semi-logarithmic scale, mean (± SD) Ch crystal and liquid crystal detection times in model biles composed of TC-, TCDC-, and MBS-L-Ch as functions of variations in CSI (1.2 to 2.4) at a constant [TL] of 7.4 g/dl (37°C, 0.15 M NaCl, pH 7.0). In all cases, detection times of ACh crystals, ChM crystals, and liquid crystals became shorter with increasing CSI values. This was particularly marked in the most pathophysiologically relevant regions **B, C** and **D** of Fig. 4 (7). Figure 12 (right panel) summarizes the influence of [TL] on mean (± SD) detection times in combined TC-, TCDC-, and MBS-L-Ch systems where the appearance of ACh and ChM crystals are progressively shortened and liquid crystal detection times are progressively prolonged with increases in [TL]. This occurred even though CSI values decreased with increasing concentration from 1.60 ± 0.04, to 1.40 ± 0.05, and to 1.17 ± 0.04, respectively.

DISCUSSION

Although precipitation of Ch crystals from supersaturated bile is the first irreversible physical-chemical step in Ch gallstone formation (1–3), it is clear that the true nucleation process has not been measured in the current work (see footnote 3). By applying the non-invasive and sensitive approach of QLS (24) as well as vitreous ice electron microscopy (D. Q-H. Wang, D. Gantz, D. M. Small, and M. C. Carey, unpublished observations) we discovered that the first precipitating particles detected in all model biles were unilamellar vesicles. Their stable $\bar{R}_h$ values of 200–1000 Å (Fig. 1) do not preclude a change in internal structure over the 0.5–168 h of measurement. As indicated in Fig. 1, vesicles gave rise quite abruptly to dramatic fluctuations in scattered light intensity that completely abrogated further measurements of particle sizes. This suggested that critical crystallization was occurring in systems with high BS/L ratios (Fig. 1) and multilamellar vesicles were forming in systems with low BS/L ratios (Figs. 2–4). The crystallization phenomena observed within the resolution limits of the light microscope took days to weeks (Fig. 3) for initiation and completion. Although these data revealed a rich and complex series of crystallization and liquid crystallization phenomena, a major reservation of our work must relate to the fact that between particle sizes of 200–1000 Å and ≈10,000 Å, i.e., from the initial time of appearances of unilamellar vesicles to microscopic solid and liquid crystals, we have no information on what physical-chemical phenomena were occurring.

Konikoff et al. (12, 14) found that thin filamentous crystals of apparently ACh (see footnote 5) crystallize from a dilute TC-rich model bile. These crystals transformed slowly through a sequence of intermediate microcrystalline structures to become classic ChM plates (12). In earlier work, two laboratories (40, 41) reported that clumps of radiating, needle-shaped crystals occurred in both model and human T-tube biles, but their significance as a habit typical of ACh was not appreciated. Collins and Phillips (42) also found that in the absence of BS, needle-shaped crystals grew from very supersaturated multilamellar vesicles of Ch and dipalmitoylphosphatidylcholine (molar ratios ≈2:1–4:1). Furthermore, earlier work using differential scanning calorimetry (43) and X-ray diffraction (44) of fresh human gallstones was strongly suggestive that ACh in addition to ChM is deposited in stones (45). Of particular interest is that scanning electron microscopy of Ch gallstones forming in guinea pigs, whose bile contains only traces of L (46), showed aggregates of needle-shaped possibly ACh and not plate-like ChM crystals (47). Collectively, these observations, together with the sequences of Kibe et al. (9) and Halpern et al. (10, 11), suggested that model and native biles may be capable of crystallizing in several different pathways.

In the present study, we explored all solid and liquid crystallization pathways systematically as functions of time and increasing L/(BS + L) ratio in model biles supersaturated by dilution. Because we investigated effects of [TL], T(°C), added Ca^{2+}, and BS hydrophobicity and proved true equilibration with termination of crystallization (Tables 3 and 4), we defined the sequences and boundaries of all crystallization pathways as well as the corresponding regions on equilibrium phase diagrams for a number of new conditions.

The most important findings in the present study were that five distinct crystallization pathways were present as functions of L/(BS + L) ratio (Figs. 3, 4). The dilute TC-rich model bile studied by Konikoff et al. (12) plotted in region **A** (Fig. 7) and had a crystallization sequence similar to what we found in the dilute TC systems. However, as noted herein, at higher [TL] and with other BS, filaments were replaced by arc-like crystals. The crystallization pathways described by Kibe and Halpern and colleagues (9–11) locate mainly to regions **C** and **D** of the current work (Fig. 4). Not fully appreciated before is that decreases in temperature (Fig. 5), [TL] (Fig. 6), and reduction in BS hydrophobicity (Fig. 7) moved all crystallization pathways and phase boundaries of the phase diagrams to the left while progressively reducing sizes of the micellar zones (Figs. 5–7). In contrast, although calcium binding to BS in mixed micelles and vesicles of bile is appreciable (48), added Ca^{2+} in the MBS-L-Ch systems had no influence on crystallization pathways, detection times, or micellar cholesterol solubilities; however, crystal number was profoundly affected (Fig. 8).

The expansion of region **E** (Fig. 4) containing liquid crystals and saturated micelles but not solid crystals with these manoeuvers has important theoretical and practical implications (35). For example, if region **E** encapsulated "physiological" lipid compositions, then it would provide a physical–chemical explanation for the delay (or absence) of ChM formation in GUDC- and TUDC-rich bile during ursodeoxycholic acid therapy of humans (49–51). It is of interest that gallbladder bile of hibernating bears can contain ≈70% TUDC (52) and, hence, if Ch-supersaturated would plot in region **E.** Contrariwise, with increasing BS hydrophobicity, all phase boundaries and crystallization pathways were shifted to the right (Fig. 7). Under these conditions, physiological bile compositions plot principally in regions **A** and **B** (Fig. 7) where ChM and ACh crystal formation are most rapid (Fig. 3). Furthermore, liquid crystals that form with physiological L/BS ratios in supersaturated TDC-rich bile are highly unstable and rapidly precipitate ChM crystals (see Results). It is interesting to note that most Ch gallstone patients have a 3- to 4-fold increase in the proportion of deoxycholate conjugates in hepatic and gallbladder biles (reviewed in refs. 53, 54) consistent with more hydrophobic BS favoring more rapid ChM crystallization under pathophysiological conditions.

In dilute or cold Ch-supersaturated model biles, liquid crystals would plot mainly in region **E** (Figs. 5 and 6) with physiological L to BS ratios thus providing an explanation why Ch crystallization seldom occurs in dilute hepatic bile despite high CSI values (55). Conversely, in concentrated gallbladder bile, Ch crystal and liquid crystal detection times are usually short (55, 56) despite lower CSI values (see Fig. 12, right panel) by virtue of a move in all phase boundaries to the right (Fig. 6). In the prairie dog, increased water and electrolyte absorption by the gallbladder occurs during early Ch gallstone formation (57), and administration of the sodium channel blocker, amiloride, greatly reduces Ch gallstone incidence by preventing increases in lipid concentration (58). Our results, therefore, provide a physical–chemical explanation for prevention of Ch gallstone formation by maintaining gallbladder bile in a dilute state and inducing physiological relative lipid compositions to plot in an expanded region **E** (Fig. 6). This is also suggested by the effects of cold on the crystallization regions in the present work (Fig. 5), in that poikilotherms would have highly stable biles, and further it is a common experience (59) that ex vivo human supersaturated biles do not crystallize easily when cold.

Although it was suggested (2) that the CSI of human bile does not act as a good predictor for the rate of ChM

crystallization, we found that higher CSI values shortened Ch crystal and liquid crystal detection times appreciably (Fig. 12, left panel) but did not influence crystallization pathways.[8] Provided that [TL] was kept constant, there was a positive correlation between higher CSI values and Ch crystal and liquid crystal detection times (Fig. 12, left panel). This effect is weakest in regions **A** and **E** and strongest in regions **C** and **D** where the relative compositions of most human biles plot (7). This suggests that higher degrees of Ch supersaturation could act as an independent pro-crystallization variable in native bile (60).

It is now well known that the addition to L, as well as changes in phospholipid class and molecular species, influence crystallization times in model and native biles (61–67). Konikoff, Cohen, and Carey (65, 67) found that in TC-rich dilute bile, saturated short-, medium-, and long-chain polyunsaturated L induced rapid precipitation of filamentous Ch crystals, indicating that the compositions plotted in region **A** of the present work (Figs. 3, 6). However, long-chain saturated L and brain sphingomyelin prolonged ChM crystallization markedly and ChM appeared before ACh crystals (65). These results indicate that with these phospholipids the model bile composition of Konikoff et al. (65) plotted in region **B** (Figs. 3, 6), suggesting that saturated L species can move phase boundary *ab* (Fig. 4) very close to the Ch axis. With respect to L content, Halpern et al. (63) and Jüngst et al. (64) demonstrated that the progressive addition of natural Ls to both model and human biles prolonged appearance times of ChM crystals; in one case, this was extended from ≈2.5 to > 21 days (64). It is clear that with changing L/(L + BS) ratios, bile compositions are produced that move through pathways **B** to **C** or **D** (Figs. 3, 11) thereby slowing the appearance times of ChM crystals. Conversely, Nervi et al. (61) found that a diet rich in legumes induced a selective reduction in biliary L content which had the opposite effect (68) and hence might be related to the high prevalence of Ch gallstones in Chileans (61, 67). Again, this is consistent with our data (Figs. 3, 11) where detection times of Ch crystals in bile were accelerated greatly by a reduction in L mole fraction below a threshold value of ≈0.13 (Fig. 11). Although it has been proposed (63, 64) that enhanced phospholipid secretion into bile may be a promising approach for preventing Ch gallstones, it is clear from the current work (Fig. 4) that prevention strategies would require bile compositions to plot in region **E** where solid Ch crystals are a forbidden phase transition and which would be difficult to achieve with MBS except in the dilute state (Fig. 6).

Our results also provide a conceptual framework for assaying effects of pro- and anti-"nucleating" factors on Ch crystallization in model or human biles (reviewed in ref. 69). For example, Ahmed et al. (70) claimed that the effects of a variety of proteins on Ch crystal formation in a TC-model bile are nonspecific, being related to protein hydrophilic–hydrophobic balance as evaluated by their elution times on a phenyl-agarose column. These authors (70) found that hydrophobic proteins inhibited whereas hydrophilic proteins enhanced Ch crystallization. The compositions of the physiologic model biles used by these authors (70) plotted in region **B** of our concentrated TC-L-Ch system (Fig. 7). Our reinterpretation of their data suggests that when hydrophilic proteins were added, the crystallization pathways became similar to those in region **A** or **B** of the current work (Fig. 7). In contrast, when hydrophobic proteins were added (70) it appeared that crystallization pathways shifted to regions **C** or **D** (Fig. 4 and 7) of the current work. These findings suggest that small amounts of proteins might shift Ch crystallization pathways (Fig. 4), and therefore might appear pro- or anti-crystallizing when the detection times of ChM crystals are measured. Furthermore, because of the upslope of the micellar phase boundary from that of pure BS to point *b* (Fig. 4) it is likely that in the metastable state, a protein that shifts crystallization pathways to the left will be associated with a redistribution of Ch from micelles in favor of vesicles, whereas a protein which shifts boundary *ab* (Fig. 4) in the opposite direction will result in a converse distribution.

The Ch-solubilizing capacity of a bile is a critical function of the hydrophobic–hydrophilic balance of the principal BS (37–39, 71). BS hydrophobicity controls capacities to solubilize Ch (37), and this is maintained in the rank order TDC > C > TCDC ≥ TC ≈MBS > GC > TUDC with all pathophysiological L contents (Fig. 10). With the more hydrophobic BS species, the micellar zones, e.g., Fig. 6 (see footnote 7), showed less concentration-dependent changes because of the low intermixed micellar/vesicular BS concentrations in these systems (72–75). The equilibrium Ch solubilities (Fig. 10) agree in large part with those obtained by us and other authors who studied model biles composed of a range of BS species (7, 76, 77). Comparing the values derived from the critical tables, with its appended correction factors (21), our experimental results show almost identical theoretical and experimental Ch solubilities in TC-L-Ch and TUDC-L-Ch systems at 37°C (Fig. 10). Furthermore, because the curves of maximal Ch solubility in both MBS-L-Ch systems with and without

[8]Theoretically, a very high CSI could influence the crystallization sequence if it induced the relative L content of the mother bile to decrease markedly during crystallization and hence induce the composition to traverse the left boundary of a crystallization pathway (see Fig. 9).

20 mM $CaCl_2$ (Fig. 8 d, inset) and TCDC-L-Ch systems approximated those of TC-L-Ch systems, the critical tables appear valid for calculating the CSIs of MBS-containing model and native biles. Whereas Ca^{2+} was known to influence phase transitions in model bile (78), its effect with the MBS-L-Ch system was not due to decreasing Ch solubility in the micellar zone (Fig. 8 d, inset) or detection times but was directly related to promoting crystal number and perhaps growth (Fig. 8).

An anticipated finding not studied systematically before (7) was that as crystallization progressed, relative lipid compositions of biles did not follow constant L to BS compositions, but rather the L fraction decreased progressively (Figs. 8 d and 9). Although predictable for regions **C, D,** and **E** where liquid crystals are a coexisting phase at equilibrium (Fig. 4), this occurred also in region **B** where liquid crystals are unexpected (Figs. 3, 4) and did not occur in region **A** as anticipated when the artefact of daily sampling for microscopy was removed (Fig. 8 d, Fig. 9). A near-constant L/BS ratio before and after crystallization suggests that unilamellar vesicles were filtered and hence ACh crystals (Figs. 2, 3) may nucleate from unilamellar vesicles in region **A.** Another implication of the L/BS ratio shift in regions **C–E** was that when relative lipid compositions were close to the boundary of a pathway (Fig. 9) and then crossed that boundary (Fig. 3) the bile appeared to renucleate according to the new crystallization pathway. This may explain, in part, some of the sequences of crystalline and liquid crystalline phenomena documented. Nonetheless in region **C** (Fig. 4), after liquid crystalline intermediates and ChM crystallization, transient appearances of ACh crystals still occurred (Fig. 3) despite mother bile compositions that remained clearly within the pathway (Fig. 9). It is notable that in earlier work, Holzbach and Marsh (79) observed variable liquid crystalline phase transitions that varied strongly with model bile composition. A reexamination of their results suggests that compositions that plotted in region **C** of Fig. 4 crossed phase boundary *ab* to lie in the left two-phase area (region **B**) where no microscopic liquid crystals form.

It is of relevance that in TC-, MBS-, and TCDC-L-Ch systems, micellar $\bar{R}_h$ values did not differ significantly between lipid concentrations of ≈6.3 (16–79 Å) and 29 g/dl (16–82 Å) for a given BS/L ratio, suggesting that the higher ionic strengths, provided principally by BS themselves, minimized micellar interactions (24). In prior work (8, 30), small decreases in micellar R_h values occurred over a more dilute range of lipid concentrations. Of greater importance is that the constancy of micellar sizes from beginning to the end of the experiments provides strong additional argument that L or Ch degradation products were not formed during the lengthy incubation periods (30 days) used. This suggests that measures used to avoid these problems were appropriate (see lipid analytic methods).

Since the current work was completed, Juste et al. (80) observed similar liquid and Ch solid crystals using supersaturated model biles containing a single lipid composition. Because BS hydrophilic–hydrophobic balance was varied by these authors (80) we determined that the crystallization sequences for TCDC-, TDC-, GCDC-, and TDC-L-Ch systems were located in region **B,** TC- and GC-L-Ch systems in region **C,** and a TUDC-L-Ch system in region **E** of the present work (Figs. 4, 7). These investigators (80) also studied a range of very hydrophilic BS species including taurohyocholate, taurohyodeoxycholate, 3α-hydroxy-6-oxo-5β-cholanoate, glycohyocholate, and glycohyodeoxycholate. Our reworking of their crystallization data (80) suggests that all crystallization pathways for the hydrophilic BS would, as anticipated (e.g., Fig. 7 TUDC-L-Ch systems (38)), plot in region **E** where liquid crystals are stable indefinitely (Figs. 4, 7).

In conclusion, we have demonstrated that five crystallization pathways are present in pathophysiologically relevant model biles as functions of increasing L fraction. Singularity of pathways and their interconversions are explained by the distinct metastable regions above the micellar zone which have now been defined explicitly. The five crystallization pathways, detection times of liquid and solid Ch crystals, and the phase boundaries of relevant phase diagrams are influenced by BS hydrophobicity, [TL], and temperature but not by CSI values[8] or added $CaCl_2$. The results help to provide rational explanations for a wide variety of disparate and often inexplicable results in the literature on the physical–chemistry of Ch crystallization in model and native biles. The present work correlates remarkably well with studies of ACh, ChM, and liquid crystallization pathways in human gallbladder bile (81) (D. Q-H. Wang and M. C. Carey, unpublished observations) and in the gallstone-susceptible inbred mouse (82) fed a lithogenic diet of dairy fat, Ch, and cholic acid (83). These studies should provide a rigorous physical–chemical basis for investigating biliary pro- and anti-crystallization and perhaps true nucleating[3] factors in native human biles and for developing phase separation inhibitors to prevent ChM precipitation.

We are greatly indebted to Dr. Donald M. Small (Boston University School of Medicine) for valuable suggestions at the initiation of this study and to Drs. Joanne M. Donovan (West Roxbury VA Medical Center) and Natasha Timofeyeva (Brigham and Women's Hospital) who carried out important preliminary studies. We also thank Ms. Monika R. Leonard and Dr. David E. Cohen (Brigham and Women's Hospital) for their help with quasi-elastic light-scattering spectroscopy and Ms. Elaine O'Rourke for superb word-processing assistance.

This work was supported in part by grants DK 36588 and DK 34854 from the National Institutes of Health (US Public Health Service).

Manuscript received 26 May 1995 and in revised form 30 November 1995.

REFERENCES

1. Small, D. M. 1980. Cholesterol nucleation and growth in gallstone formation. *N. Engl. J. Med.* **302:** 1305–1307.
2. Holan, K. R., R. T. Holzbach, R. E. Hermann, A. M. Cooperman, and W. J. Claffey. 1979. Nucleation time: a key factor in the pathogenesis of cholesterol gallstone disease. *Gastroenterology.* **77:** 611–617.
3. Sedaghat, A., and S. M. Grundy. 1980. Cholesterol crystals and the formation of cholesterol gallstones. *N. Engl. J. Med.* **302:** 1274–1277.
4. Carey, M. C. 1996. Formation and growth of cholesterol gallstones: the new synthesis. In Bile Acids, Cholestasis-Gallstones. H. Fromm and U. Leuschner, editors. Kluwer, Dordrecht. 147–175.
5. Bourgès, M. C., D. M. Small, and D. G. Dervichian. 1967. Biophysics of lipid associations. III. The quaternary systems lecithin–bile salt–cholesterol–water. *Biochim. Biophys. Acta.* **144:** 189–201.
6. Holzbach, R. T., M. Marsh, M. Olszewski, and K. Holan. 1973. Cholesterol solubility in bile. Evidence that supersaturated bile is frequent in healthy man. *J. Clin. Invest.* **52:** 1467–1479.
7. Carey, M. C., and D. M. Small. 1978. The physical chemistry of cholesterol solubility in bile. Relationship to gallstone formation and dissolution in man. *J. Clin. Invest.* **61:** 998–1026.
8. Mazer, N. A., and M. C. Carey. 1983. Quasi-elastic light-scattering studies of aqueous biliary lipid systems. Cholesterol solubilization and precipitation in model bile solutions. *Biochemistry.* **22:** 426–442.
9. Kibe, A., M. A. Dudley, Z. Halpern, M. P. Lynn, A. C. Breuer, and R. T. Holzbach. 1985. Factors affecting cholesterol monohydrate crystal nucleation time in model systems of supersaturated bile. *J. Lipid Res.* **26:** 1102–1111.
10. Halpern, Z., M. A. Dudley, M. P. Lynn, J. M. Nader, A. C. Breuer, and R. T. Holzbach. 1986. Vesicle aggregation in model systems of supersaturated bile: relation to crystal nucleation and lipid composition of the vesicular phase. *J. Lipid Res.* **27:** 295–306.
11. Halpern, Z., M. A. Dudley, A. Kibe, M. P. Lynn, A. C. Breuer, and R. T. Holzbach. 1986. Rapid vesicle formation and aggregation in abnormal human biles. A time-lapse video-enhanced contrast microscopy study. *Gastroenterology.* **90:** 875–885.
12. Konikoff, F. M., D. S. Chung, J. M. Donovan, D. M. Small, and M. C. Carey. 1992. Filamentous, helical, and tubular microstructures during cholesterol crystallization from bile. Evidence that cholesterol does not nucleate classic monohydrate plates. *J. Clin. Invest.* **90:** 1155–1160.
13. Chung, D. S., G. B. Benedek, F. M. Konikoff, and J. M. Donovan. 1993. Elastic free energy of anisotropic helical ribbons as metastable intermediates in the crystallization of cholesterol. *Proc. Natl. Acad. Sci. USA.* **90:** 11341–11345.
14. Konikoff, F. M., and M. C. Carey. 1994. Cholesterol crystallization from a dilute bile salt-rich model bile. *J. Cryst. Growth.* **144:** 79–86.
15. Shieh, H. S., L. G. Hoard, and C. E. Nordman. 1977. Crystal structure of anhydrous cholesterol. *Nature (London).* **267:** 287–289.
16. Harvey, R. C., D. Taylor, C. N. Petrunka, A. D. Murray, and S. M. Strasberg. 1985. Quantitative analysis of major, minor and trace elements in gallbladder bile of patients with and without gallstones. *Hepatology.* **5:** 129–132.
17. Pope, J. L. 1967. Crystallization of sodium taurocholate. *J. Lipid Res.* **8:** 146–147.
18. Vercaems, R., A. Union, and M. Rossenen. 1989. Separation and quantitation of free cholesterol and cholesteryl esters in a macrophage cell line by high performance liquid chromatography. *J. Chromatogr.* **494:** 43–52.
19. Hoffman, L. M., W. Fok, and L. Schneck. 1974. Quantitative determination of lysolecithin and sphingomyelin in phospholipid mixtures by thin-layer chromatography as applied to the thymus of fm/fm mouse. *J. Lipid Res.* **15:** 283–285.
20. Igimi, H., and M. C. Carey. 1981. Cholesterol gallstone dissolution in bile: dissolution kinetics of crystalline (anhydrate and monohydrate) cholesterol with chenodeoxycholate, ursodeoxycholate, and their glycine and taurine conjugates. *J. Lipid Res.* **22:** 254–270.
21. Carey, M. C. 1978. Critical tables for calculating the cholesterol saturation of native bile. *J. Lipid Res.* **19:** 945–955.
22. Hofmann, A. F. 1976. The enterohepatic circulation of bile acid in man. *Adv. Intern. Med.* **21:** 501–534.
23. Staggers, J. E., O. Hernell, R. J. Stafford, and M. C. Carey. 1990. Physical-chemical behavior of dietary and biliary lipids during intestinal digestion and absorption. 1. Phase behavior and aggregation states of model lipid systems patterned after aqueous duodenal contents of healthy adult human beings. *Biochemistry.* **29:** 2028–2040.
24. Cohen, D. E., M. R. Fisch, and M. C. Carey. 1990. Principles of laser light-scattering spectroscopy: applications to the physicochemical study of model and native biles. *Hepatology.* **12:** 113S–122S.
25. Renshaw, P. F., A. S. Janoff, and K. W. Miller. 1983. On the nature of dilute aqueous cholesterol suspensions. *J. Lipid Res.* **24:** 47–51.
26. Craven, B. M. 1976. Crystal structure of cholesterol monohydrate. *Nature (London).* **260:** 727–729.
27. Turley, S. D., and J. M. Dietschy. 1978. Re-evaluation of the 3α-hydroxysteroid dehydrogenase assay for total bile acids in bile. *J. Lipid Res.* **19:** 924–928.
28. Bartlett, G. R. 1959. Phosphorous assay in column chromatography. *J. Biol. Chem.* **234:** 466–468.
29. Fromm, H., P. Amin, H. Klein, and I. Kupke. 1980. Use of a simple enzymatic assay for cholesterol analysis in human bile. *J. Lipid Res.* **21:** 259–261.
30. Mazer, N. A., G. B. Benedek, and M. C. Carey. 1980. Quasielastic light-scattering studies of aqueous biliary lipid systems. Mixed micelle formation in bile salt-lecithin solutions. *Biochemistry.* **19:** 601–615.
31. Juniper, K., Jr., and E. N. Burson, Jr. 1957. Biliary tract studies. II. The significance of biliary crystals. *Gastroenterology.* **32:** 175–208.
32. Loomis, C. R., G. G. Shipley, and D. M. Small. 1979. The phase behavior of hydrated cholesterol. *J. Lipid Res.* **20:** 525–535.
33. Rosevear, F. B. 1954. The microscopy of the liquid crystalline neat and middle phases of soaps and synthetic detergents. *J. Am. Oil Chem. Soc.* **31:** 628–639.

34. Small, D. M., M. C. Bourgès, and D. G. Dervichian. 1966. The biophysics of lipidic associations. I. The ternary systems lecithin–bile salt–water. *Biochim. Biophys. Acta.* **125:** 563–580.
35. Carey, M. C., and D. E. Cohen. 1987. Biliary transport of cholesterol in vesicles, micelles and liquid crystals. *In* Bile Acids and the Liver. G. Paumgartner, A. Stiehl, and W. Gerok, editors. MTP Press, Lancaster. 287–300.
36. Cohen, D. E., and M. C. Carey. 1991. Acyl chain unsaturation modulates distribution of lecithin molecular species between mixed micelles and vesicles in model bile. Implications for particle structure and metastable cholesterol solubilities. *J. Lipid Res.* **32:** 1291–1302.
37. Armstrong, M. J., and M. C. Carey. 1982. The hydrophobic–hydrophilic balance of bile salts. Inverse correlation between reverse-phase high performance liquid chromatographic mobilities and micellar cholesterol-solubilizing capacities. *J. Lipid Res.* **23:** 70–80.
38. Carey, M. C. 1988. Lipid solubilization in bile. *In* Bile Acids in Health and Disease. T. C. Northfield, R. P. Jazrawi, and P. L. Zentler-Munro, editors. Kluwer, Dordrecht. 61–82.
39. Salvioli, G., H. Igimi, and M. C. Carey. 1983. Cholesterol gallstone dissolution in bile. Dissolution kinetics of crystalline cholesterol monohydrate by conjugated chenodeoxycholate-lecithin and conjugated ursodeoxycholate-lecithin mixtures: dissimilar phase equilibria and dissolution mechanisms. *J. Lipid Res.* **24:** 701–720.
40. Toor, E. W., D. F. Evans, and E. L. Cussler. 1978. Cholesterol monohydrate growth in model bile solutions. *Proc. Natl. Acad. Sci. USA.* **75:** 6230–6234.
41. Lichtenberg, D., S. Ragimova, A. Bor, S. Almog, C. Vinkler, M. Kalina, Y. Peled, and Z. Halpern. 1988. Stability of mixed micellar bile models supersaturated with cholesterol. *Biophys. J.* **54:** 1013–1025.
42. Collins, J. J., and M. C. Phillips. 1982. The stability and structure of cholesterol-rich codispersions of cholesterol and phosphatidylcholine. *J. Lipid Res.* **23:** 291–298.
43. Dubler, E., and B. Kamber. 1980. Thermal analysis of biogenic solid compounds. *In* Thermal Analysis. Proceedings of 6th International Conference on Thermal Analysis (Bayreuth). Birkhäuser, Basel. 531–539.
44. Aho, A. J., E. Vilhonen, S. Peltola, and A. Lehtonen. 1985. An X-ray diffraction study of the crystalline composition of gallstones. *Scand. J. Gastroenterol.* **20:** 901–906.
45. Hsu, L-Y., and C. E. Nordman. 1983. Phase transition and crystal structure of the 37°C form of cholesterol. *Science.* **220:** 604–606.
46. Holzbach, R. T., M. E. Marsh, and M. C. Hallberg. 1971. The effect of pregnancy on lipid composition of guinea pig gallbladder bile. *Gastroenterology.* **60:** 288–293.
47. Jenkins, S. A. 1978. Biliary lipids, bile acids and gallstone formation in hypovitaminotic C guinea-pigs. *Br. J. Nutr.* **40:** 317–322.
48. Donovan, J. M., M. R. Leonard, A. K. Batta, and M. C. Carey. 1994. Calcium affinity for biliary lipid aggregates in model biles: complimentary importance of bile salts and lecithin. *Gastroenterology.* **107:** 831–846.
49. Hirota, I., K. Chijiiwa, H. Noshiro, and F. Nakayama. 1992. Effect of chenodeoxycholate and ursodeoxycholate on nucleation time in human gallbladder bile. *Gastroenterology.* **102:** 1668–1674.
50. Sahlin, S., J. Ahlberg, B. Angelin, E. Reihnér, and K. Einarsson. 1991. Nucleation time of gall bladder bile in gall stone patients: influence of bile acid treatment. *Gut.* **32:** 1554–1557.
51. Tazuma, S., H. Sasaki, S. Mizuno, H. Sagawa, S. Hashiba, I. Horiuchi, and G. Kajiyama. 1989. Effect of ursodeoxycholic acid administration on nucleation time in human gallbladder bile. *Gastroenterology.* **97:** 173–178.
52. Hagey, L. R., D. L. Crombie, E. Espinosa, M. C. Carey, H. Igimi, and A. F. Hofmann. 1993. Ursodeoxycholic acid in the Ursidae: biliary bile acids of bears, pandas, and related carnivors. *J. Lipid Res.* **34:** 1911–1917.
53. Marcus, S. N., and K. W. Heaton. 1988. Deoxycholic acid and the pathogenesis of gall stones. *Gut.* **29:** 522–533.
54. Carey, M. C., and J. T. LaMont. 1992. Cholesterol gallstone formation. 1. Physical–chemistry of bile and biliary lipid secretion. *Prog. Liver Dis.* **10:** 139–163.
55. Gollish, S. H., M. J. Burnstein, R. G. Ilson, C. N. Petrunka, and S. M. Strasberg. 1983. Nucleation of cholesterol monohydrate crystals from hepatic and gallbladder bile of patients with cholesterol gall stones. *Gut.* **24:** 836–844.
56. van Erpecum, K. J., G. P. van Berge Henegouwen, B. Stoelwinder, Y. M. G. Schmidt, and F. L. H. Willekens. 1990. Bile concentration is a key factor for nucleation of cholesterol crystals and cholesterol saturation index in gallbladder bile of gallstone patients. *Hepatology.* **11:** 1–6.
57. Conter, R. L., J. J. Roslyn, V. Porter-Fink, and L. Den-Besten. 1986. Gallbladder absorption increases during early cholesterol gallstone formation. *Am. J. Surg.* **151:** 184–191.
58. Strichartz, S. D., M. Z. Abedin, M. S. Abdou, and J. J. Roslyn. 1989. The effects of amiloride on biliary calcium and cholesterol gallstone formation. *Ann. Surg.* **209:** 152–156.
59. Vlahcevic, Z. R., C. C. Bell, Jr., P. Juttijudata, and L. Swell. 1971. Bile-rich duodenal fluid as an indicator of biliary lipid composition and its applicability to detection of lithogenic bile. *Am. J. Dig. Dis.* **16:** 797–802.
60. Sahlin, S., J. Ahlberg, B. Angelin, S. Ewerth, K. Nilsell, E. Reihnér, and K. Einarsson. 1988. Occurrence of cholesterol monohydrate crystals in gallbladder and hepatic bile in man: influence of bile acid treatment. *Eur. J. Clin. Invest.* **18:** 386–390.
61. Nervi, F., C. Covarrubias, P. Bravo, N. Velasco, N. Ulloa, F. Cruz, M. Fava, C. Severin, R. Del Pozo, C. Antezana, V. Valdivieso, and A. Arteaga. 1989. Influence of legume intake on biliary lipids and cholesterol saturation in young Chilean men. *Gastroenterology.* **96:** 825–830.
62. Booker, M. L., W. W. LaMorte, S. A. Ahrendt, K. D. Lillemoe, and H. A. Pitt. 1992. Distribution of phosphatidylcholine molecular species between mixed micelles and phospholipid-cholesterol vesicles in human gallbladder bile: dependence on acyl chain length and unsaturation. *J. Lipid Res.* **33:** 1485–1492.
63. Halpern, Z., M. Moshkowitz, H. Laufer, Y. Peled, and T. Gilat. 1993. Effect of phospholipids and their molecular species on cholesterol solubility and nucleation in human and model biles. *Gut.* **34:** 110–115.
64. Jüngst, D., T. Lang, P. Huber, V. Lange, and G. Paumgartner. 1993. Effect of phospholipids and bile acids on cholesterol nucleation time and vesicular/micellar cholesterol in gallbladder bile of patients with cholesterol stones. *J. Lipid Res.* **34:** 1457–1464.
65. Konikoff, F. M., D. E. Cohen, and M. C. Carey. 1994. Phospholipid molecular species influence crystal habits and transition sequences of metastable intermediates dur-

ing cholesterol crystallization from bile salt-rich model bile. *J. Lipid Res.* **35:** 60–70.
66. Hay, D. W., M. J. Cahalane, N. Timofeyeva, and M. C. Carey. 1993. Molecular species of lecithins in human gallbladder bile. *J. Lipid Res.* **34:** 759–768.
67. Konikoff, F. M., D. E. Cohen, and M. C. Carey. 1994. Filamentous crystallization of cholesterol and its dependence on lecithin species in bile. *Mol. Cryst. Liq. Cryst.* **248:** 291–296.
68. Grundy, S. M. 1989. Role of biliary phospholipids in cholesterol gallstone formation. *Gastroenterology.* **96:** 942–943.
69. LaMont, J. T., and M. C. Carey. 1992. Cholesterol gallstone formation. 2. Pathobiology and pathomechanics. *Prog. Liver Dis.* **10:** 165–191.
70. Ahmed, H. A., M. L. Petroni, M. Abu-Hamdiyyah, R. P. Jazrawi, and T. C. Northfield. 1994. Hydrophobic/hydrophilic balance of proteins: a major determinant of cholesterol crystal formation in model bile. *J. Lipid Res.* **35:** 211–219.
71. Donovan, J. M., N. Timofeyeva, and M. C. Carey. 1989. Cholesterol monohydrate and liquid crystal formation in model biles: effects of bile salt hydrophobicity and phosphatidylcholine contents. *Hepatology.* **10:** 598 (Abstract).
72. Duane, W. C. 1975. The intermicellar bile salt concentration in equilibrium with the mixed micelles of human bile. *Biochim. Biophys. Acta.* **398:** 275–286.
73. Duane, W. C. 1977. Taurocholate- and taurochenodeoxycholate-lecithin micelles: the equilibrium of bile salt between aqueous phase and micelle. *Biochim. Biophys. Res. Commun.* **74:** 223–229.
74. Donovan, J. M., N. Timofeyeva, and M. C. Carey. 1991. Influence of total lipid concentration, bile salt:lecithin ratio, and cholesterol content on inter-mixed micellar/vesicular (non-lecithin-associated) bile salt concentrations in model bile. *J. Lipid Res.* **32:** 1501–1512.
75. Donovan, J. M., A. A. Jackson, and M. C. Carey. 1993. Molecular species composition of inter-mixed micellar/vesicular bile salt concentrations in model bile: dependence upon hydrophilic-hydrophobic balance. *J. Lipid Res.* **34:** 1131–1140.
76. Hegardt, F. G., and H. Dam. 1971. The solubility of cholesterol in aqueous solutions of bile salts and lecithin. *Z. Ernahrungswiss.* **10:** 223–233.
77. Tamesue, N., T. Inoue, and K. Juniper, Jr. 1973. Solubility of cholesterol in bile salt-lecithin model systems. *Am. J. Dig. Dis.* **18:** 670–678.
78. Berenson, M. M., and J. R. Cardinal. 1985. Calcium accelerates cholesterol phase transitions in analog bile. *Experientia.* **41:** 1328–1330.
79. Holzbach, R. T., and M. Marsh. 1974. Transient liquid crystals in human bile analogues. *Mol. Cryst. Liq. Cryst.* **28:** 217–222.
80. Juste, C., I. Catala, R. Henry, C. Chabanet, A-M. Gueugneau, F. Béguet, B. Lyan, and T. Corring. 1995. Influence of bile salt molecular species on cholesterol crystallization from supersaturated model biles. *Biochim. Biophys. Acta.* **1254:** 89–97.
81. Wang, D. Q-H., and M. C. Carey. 1995. Cholesterol crystal nucleation paths in human gallbladder bile are identical to model bile: increased secondary bile salts and cholesterol saturation index are partly responsible for accelerating cholesterol nucleation. *Gastroenterology.* **108:** A1196.
82. Khanuja, B., Y-C. Cheah, M. Hunt, P. M. Nishina, D. Q-H. Wang, H. W. Chen, J. T. Billheimer, M. C. Carey, and B. Paigen. 1995. *Lith 1,* a major gene affecting cholesterol gallstone formation among inbred strains of mice. *Proc. Natl. Acad. Sci. USA.* **92:** 7729–7733.
83. Wang, D. Q-H., B. Paigen, and M. C. Carey. 1995. Phenotypic characterization of *Lith* genes determining susceptibility to cholesterol gallstone formation in inbred mice. *Hepatology.* **22:** 289A.